Polyethylene Oxide Chain Density and Uremic Toxin Effects on Plasma Protein Adsorption

by

Aishwarya Shrikrishna Pawar

A thesis submitted in partial fulfillment of the requirements for the degree of

Master of Science

in

Chemical Engineering

Department of Chemical and Materials Engineering

University of Alberta

Abstract

Protein adsorption to implanted biomaterials can direct host responses and lead to health complications and device failure. Polyethylene oxide (PEO) is the gold standard film for reducing non-specific protein adsorption. Although polymer chain density is an important factor in determining PEO's protein-resistant behavior, limited studies have related PEO chain density changes to the adsorption of plasma proteins. Besides, existing literature on protein adsorption primarily offers insights from the use of blood from healthy donors, neglecting changes in the blood that occur in unhealthy patients. In chronic kidney disease (CKD), uremic toxins (UTXs) accumulate in the blood compartment and significantly alter the blood composition. For the advancement of low-fouling surfaces for blood-contacting biomaterials and in the quest for personalized dialysis, addressing this knowledge gap is necessary. To examine this, PEO films with variable chain densities and two different end groups, methoxy ($-OCH_3$) and hydroxy (-OH), were prepared and characterized using dynamic contact angle, ellipsometry, and X-ray photoelectron spectroscopy (XPS), to confirm the successful deposition of PEO. Protein adsorption experiments were conducted using human plasma with and without UTXs to investigate their effect on protein adsorption. It was observed that fibrinogen, albumin, factor XI, complement C3, and IgG were the major proteins detected on both methoxy and hydroxy-PEO-modified films. The addition of UTXs substantially increased protein adsorption to methoxy-terminated PEO films, whereas no specific trend was observed for hydroxy-PEO films. The effect of chain densities did not exhibit a consistent pattern but significantly affected the adsorption of many proteins. This knowledge is integral to developing the standard protein adsorption profile and subsequent advancement of surface technologies that enable personalized treatment strategies for patients with kidney failure.

Preface

This thesis is an original work by Aishwarya Pawar and was conducted under the supervision of Dr. Larry D. Unsworth, who contributed to concept development and manuscript revisions throughout. The research detailed in this document was performed at the Department of Chemical and Materials Engineering, University of Alberta, North Campus, Canada. The experiments involving human plasma were conducted in accordance with approved research ethics board approvals: Canadian Blood Services 2022-21 and University of Alberta Pro00002363 and Pro00116764. With the exception of the data collection presented in Chapters 3.3.3 and 4.3.3, which were obtained from experiments conducted by the Nanofab facility at the University of Alberta, all data collection and analysis throughout this thesis constitutes my original work.

Content from Chapter 3 has been presented as an abstract titled "Biocompatibility of PEO-Gold Surfaces in Chronic Kidney Disease Patients: A Study by Western Blotting" at the CSPS-CC-CRS Symposium 2024, held from June 10 to 14, 2024. An abstract titled "Western Blot Analysis of Metabolite Effects on Protein Adsorption to PEO Gold Surfaces," including content from Chapters 3 and 4, was presented at the Faculty of Engineering Graduate Research Symposium (FEGRS) 2024, held from August 13 to 15, 2024. Chapter 3 is currently under review as 'Effect of uremic toxins and methoxy-PEO chain density on plasma protein adsorption' in ACS Biomaterials Science & Engineering. Chapter 4 has been submitted as 'Effect of hydroxy-PEO chain density and uremic toxins on plasma protein adsorption' in Colloids and Surfaces B: Biointerfaces.

Acknowledgment

My heartfelt gratitude to my supervisor, Dr. Larry D. Unsworth, for his unwavering support and guidance. His patience, encouragement, and insightful feedback were instrumental in ensuring the smooth progress of this project.

My sincere thanks to Dr. Mehdi Ghaffari Sharaf for his constant availability and support, as well as to my lab mate, Miss Ayda Ghahramanzadeh, for her valuable cooperation. I express my affectionate regards to my cherished friends and mentors. Their profound insights and invaluable advice have greatly enriched my research journey.

Finally, this endeavor would not have been possible without the unwavering emotional and moral support of my loving parents, Mrs. Saraswati Pawar and Mr. Shrikrishna Pawar. Their steadfast encouragement and understanding have been invaluable. My heartfelt thanks are further extended to my grandfather, Mr. Vishnu Dhane, for always believing in me and making my research journey possible.

Table of contents

List of Tables

List of Figures

Chapter 1. Introduction

1.1 Host responses to biomaterials

Biomaterial implantation in a body causes the material surface to interact extensively with surrounding tissues, especially blood and its components. At this early stage, the biomaterial interacts with the inflammatory or immune cells, a multitude of proteins present in the blood, and small metabolites (<1000 Da), which include numerous components of cellular functions [1, 2]. The materials rapidly develop an adsorbed protein layer, typically before the arrival of inflammatory or immune cells [2]. Metabolites exhibit interaction patterns similar to those of proteins [1], however, considering the generation of host responses, protein adsorption is the primary and fate determining step. Protein-biomaterial interactions are sometimes purposeful and essential to the biomaterial's design and function. However, unfavorable interactions, most importantly non-specific protein adsorption, lead to host responses including thrombosis and immune responses such as frustrated phagocytosis and complement activation, which reduce the functionality and lifespan of the biomaterial [3, 4]. These responses are inadequately controlled by the host's natural regulatory systems, such as fibrinolysis. Moreover, the mechanisms underlying protein adsorption and corresponding host responses remain largely unclear. Therefore, understanding these mechanisms is important in developing strategies to ensure hemocompatibility and functionality of the device in situ.

1.1.1. Protein adsorption mechanisms

The interactions between surface and protein are complex due to the involvement of several factors: the variation in surface materials, diversity in proteins present in the blood, the dynamic nature of adsorbed proteome on a biomaterial surface, and change in proteins' structure upon adsorption that leads to further host reactions [5, 6]. The multitude of plasma proteins adsorbed to a surface is called as adsorbed proteome, from which we have screened a small subset in this study. At the start, protein adsorption is primarily governed by diffusion. However, as time goes on, the affinity of proteins for the surface plays a vital role, leading to the replacement of high-concentration low-affinity proteins by those with low-concentration high-affinity proteins [6]. Proteins, with their acidic (-COOH) and basic ($-NH_2$) groups, can be positively, negatively, or neutrally charged. The non-polar domains of proteins are highly sensitive to variations in temperature, pH, ionic strength, or interactions with a surface. Proteins are surface-active due to their amphiphilic and macromolecular properties and possess a strong affinity towards any interface [7]. The protein adsorption to biomaterials is also driven by the hydrophobic effect [7], where non-polar regions of proteins can self-associate to minimize contact with water, leading the proteins to adsorb on surfaces. Interfacial forces such as electrostatic and van der Waals interactions between surface and bulk also play a crucial role in protein adsorption to surfaces [8-10]. It has been found that the interfacial forces are active at an average distance of 10 nm to favor protein adsorption to the surfaces [7]. Depending on the charges on surfaces and proteins, electrostatic interactions can facilitate non-specific protein adsorption. The fundamental surface properties, including wettability, topography, charge, and chemistry, have also been recorded to influence protein adsorption [11]. The increased hydrophobicity and surface roughness, and opposite charges between surface and proteins tend to increase protein adsorption [11]. Moreover,

the functional groups on the material surface facilitate the adsorption of specific proteins [11]. For example, the methyl (-CH_3) group binds to fibrinogen and IgG, the hydroxy (-OH) and amine (-NH_2) groups bind to fibronectin, and the carboxylic acid (-COOH) group binds to fibronectin and albumin.

1.1.2. Material-induced thrombogenesis

The coagulation system plays a vital role in upholding a closed, high-pressure circulatory system [12, 13]. Effective hemostasis, which is essential to stop bleeding, depends on the proper activation of coagulation in response to vascular injury [12]. The rapid adsorption of plasma proteins onto artificial surfaces can lead to thrombus formation, which then alters the course of subsequent reactions, including blood coagulation [14]. The presence of biomaterials like vascular grafts, hemodialyzers, catheters, membrane oxygenators, and several polymeric biomaterials [15-20] can cause aberrant coagulation that leads to several thrombotic disorders and reduces biomaterial function [12].

1.1.2.1 Contact pathway of coagulation

The multiprotein coagulation cascade involves two distinct pathways: the extrinsic (the tissue factor) and the intrinsic (contact-mediated) pathway, which converge to progress into the common pathway (Figure 1.1).

The principal components of an extrinsic pathway include the transmembrane receptor tissue factor (TF) and plasma factor VII [5, 21]. In abnormal physiological conditions such as tissue damage or injury, tissue factor (TF) is continuously expressed by damaged cells. Under such conditions, plasma factor VII gets activated to factor VIIa and binds to tissue factor, thereby

beginning the clotting process. This complex further binds to factor X and enters the common pathway.

The intrinsic pathway [5, 12], however, is of greater relevance to this research, given that it does not involve tissue damage. It begins with the activation of factor XII upon exposure to negatively charged molecules and protein adsorption to surfaces. Activated factor XII (factor XIIa) converts prekallikrein to kallikrein and, with the help of high molecular weight kininogen (HMWK), activates factor XI to factor XIa. Factor XIa activates factor IX to IXa, which further activates factor X, eventually entering the common pathway.

Once factor X is activated by either extrinsic or intrinsic pathway, it converts prothrombin to thrombin. Thrombin is a potential fibrinolytic enzyme that cleaves fibrinogen to fibrin. The repeated binding of fibrin to fibrin-stabilizing factor XIIIa ultimately creates a stable fibrin clot [14].

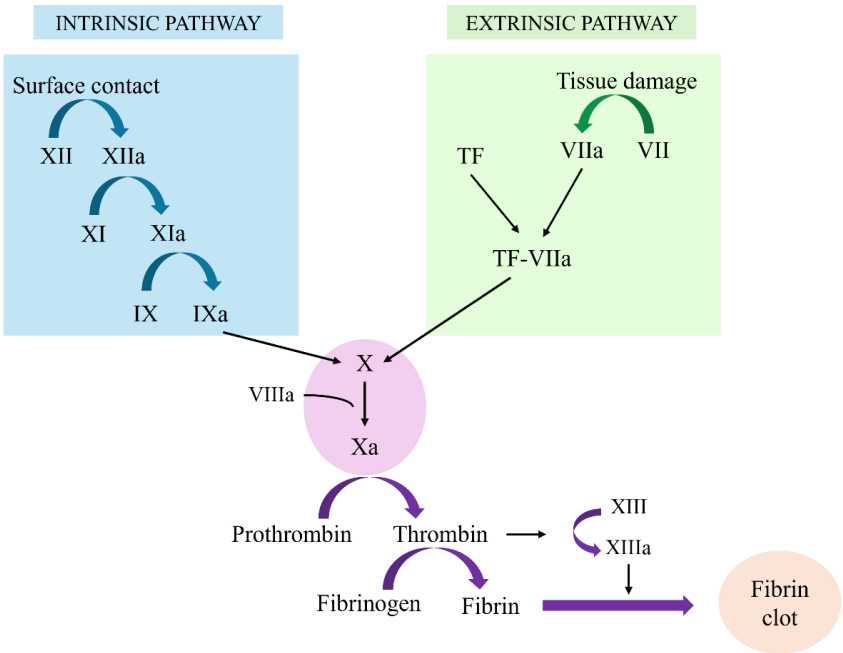

Figure 1.1 Intrinsic and extrinsic coagulation activation pathways. The figure reproduced with permission from [22].

1.1.2.2 Regulation of thrombogenesis *via* fibrinolysis

Maintaining a precise balance between thrombogenesis and fibrinolysis is essential to hemostasis. This balance is regulated by numerous activators and controlling factors throughout the different pathways. Several blood proteins, for example, plasminogen, degrade fibrin clots after the damage is repaired and release the cellular components in the bloodstream (Figure 1.2) [23]. Fibrin clot surfaces are critical activation sites for fibrinolysis and facilitate the interaction of plasminogen and plasmin [24]. Fibrinolysis is initiated by plasminogen activators, tPA (tissue plasminogen activator) or uPA (urokinase plasminogen activator), which convert plasminogen to plasmin [25]. While tPA necessitates its binding to fibrin to function more efficiently, [26], uPA can activate plasminogen independent of fibrin in the fluid phase [27]. The amplification of generated fibrinolysis is performed by α_2-antiplasmin, a serine protease inhibitor that binds to fibrin and protects it from inhibition. Both fibrin and fibrinogen promote the conversion of plasminogen to plasmin, thereby inadvertently accelerating their own breakdown [28]. As tPA and uPA are short-lived, with a half-life of 4-8 minutes in circulation, several plasminogen receptors on cell surfaces bind to plasminogen to continue fibrinolysis [28]. In addition to plasminogen, other blood proteins, including antithrombin, protein S, and protein C, regulate coagulation by acting as anticoagulants.

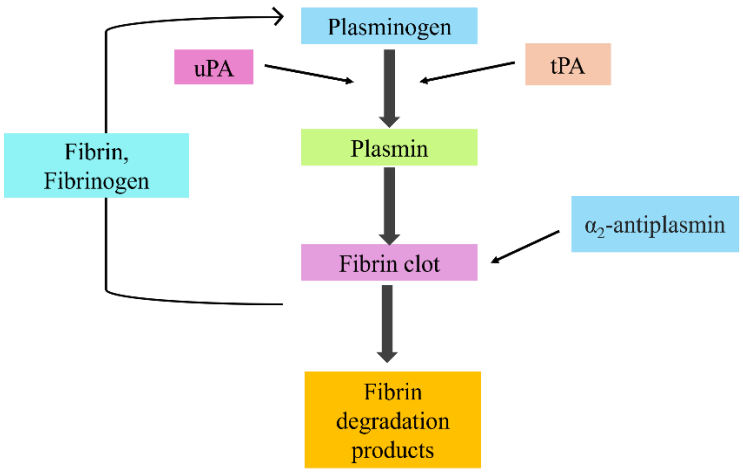

Figure 1.2 Schematic representation of degradation of fibrin clot.

1.1.3. Biomaterial-induced immune response

The immune system is a complex system that defends the host against foreign invaders such as microbes, viruses, parasites, and foreign materials, including biomaterials. It is divided into two categories: innate and adaptive immune responses. Innate immunity immediately responds to all foreign bodies upon detection and consists of protein-based humoral elements, physical barriers, inflammation, and cells like neutrophils and macrophages [5]. Adaptive immune responses are delayed compared to innate responses but are specific to the foreign body type. Furthermore, adaptive immunity maintains a memory of past foreign entities, enabling a quicker host response when reintroduced to pathogens [5].

1.1.3.1 Innate immunity

A crucial protein-based element of the innate immune system is the complement system. Upon detection of foreign surfaces, basically, through the complement proteins' adsorption, the complement system is activated and results in inflammation, opsonization, and eventually cell-lysis [5]. The complement system is activated by three significant pathways: classical, alternative,

and mannose-binding lectin pathway (Figure 1.3). The classical activation pathway, being the antibody-dependent mechanism of complement activation, holds some relevance for the biomaterials-generated immune responses, however, its contribution is not very significant [5]. The lectin pathway depends on the recognition of carbohydrates on the pathogen surface and is not significant in complement activation by biomaterials until the biomaterials are modified with these reagents [29].

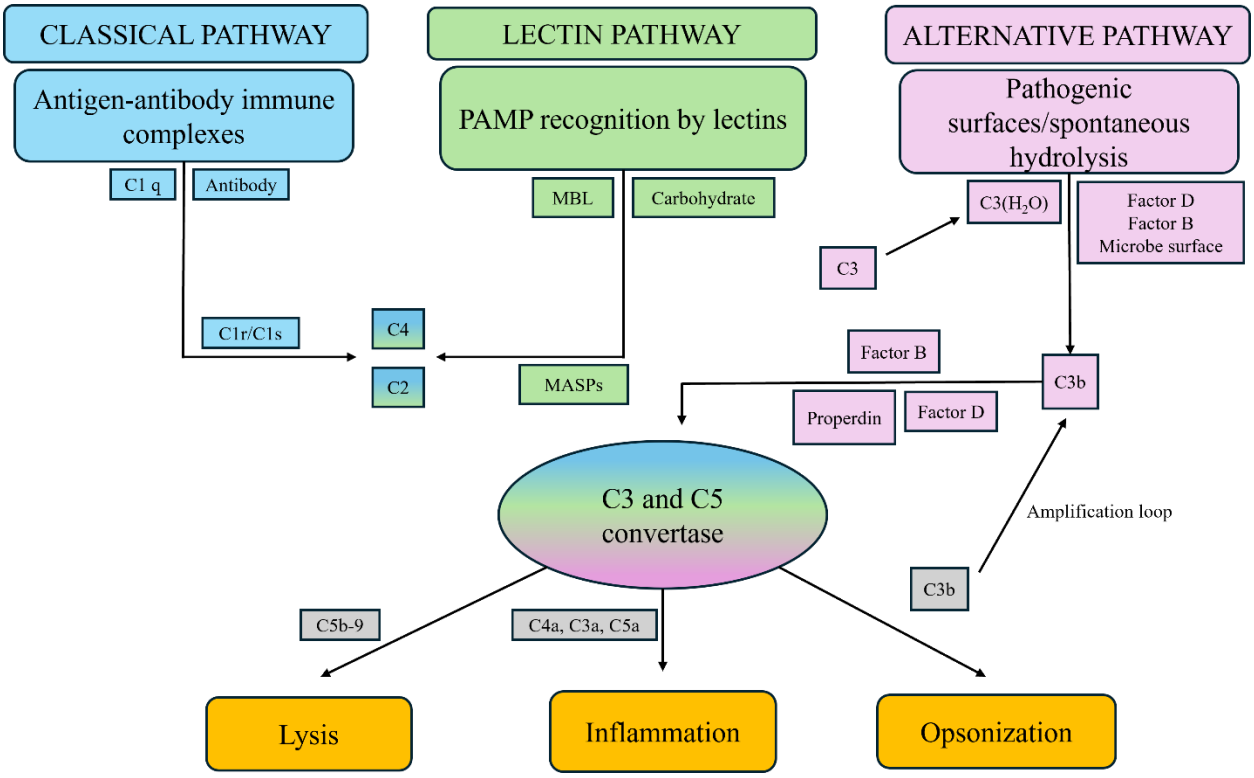

Figure 1.3. Classical, alternative, and mannose-binding lectin pathways of complement activation. Image reproduced from Dunkelberger et. al. [29] © Cell Research, 2010

Alternative pathway plays the most significant role in biomaterial-induced complement activation [30]. The complement activation by the alternative pathway is non-specific, and instead of recognizing specific antigens or carbohydrates, it functions through the accumulation of spontaneously generated C3b on a biomaterial surface [5]. It begins with the complement C3 hydrolysis to C3(H_2O). C3(H_2O), with the help of factor D, cleaves factor B into Bb and Ba and forms the initial C3 convertase [31]. This initial C3 convertase forms an amplification loop and begins breaking down C3 into C3a and C3b. The C3b generated here can directly bind to surfaces and, with the aid of factor B and factor D, can generate the predominant C3 convertase. Properdin (factor P) stabilizes this complex and amplifies the alternative pathway activation [29, 32]. The non-specific complement activation has been noticed to impact the host health in patients undergoing hemodialysis and cardiopulmonary bypass. It was observed that the biomedical devices implanted to treat these diseases were capable of generating complement activation through an alternative pathway [5, 33].

Considering the seriousness of its consequences, it is crucial to regulate the alternative complement response generated by biomaterials. Complement factor I (CFI) and Complement factor H (CFH) are the central plasma regulators of the alternative pathway [34]. Absence or dysfunction of either factor leads to excessive activation of the complement, causing overutilization of complement components such as C3, leading to secondary complement deficiency. CFI is a serine protease in plasma that irreversibly converts C3b to inactive C3b (iC3b) through proteolysis. CFI further breaks iC3b into secondary breakdown products, C3dg and C3c, with the aid of cofactors such as CFH – a single-chain glycoprotein. CFH independently controls complement activation by acting as a competitor of factor B to bind C3b, dissociating C3b and Bb, and deactivating alternative pathway C3 convertase.

1.1.3.2 Adaptive immunity

This form of immunity comprises cellular components, circulating proteins, and cytokines produced by cells. More specifically, the family of immunoglobulins is the primary humoral protein component of adaptive immunity. Immunoglobulin G (IgG) stands out as the most prevalent among the five major immunoglobulin groups. IgG consists of four polypeptide chains with two pairs of identical protein chains called heavy and light chains. IgG binds to an antigen and triggers the recruitment of macrophages or natural killer cells to opsonize and degrade the pathogen. The adsorption of IgG to biomaterial surfaces initiates these immune responses and may lead to compromised device performance or even failure. As a result, the host can suffer from frustrated phagocytosis, formation of foreign-body giant cells (fused macrophages) that leads to an acellular collagen barrier formation [35].

Numerous other proteins in human plasma are involved in generating and maintaining immune responses [23]. Vitronectin functions as a crucial component in regulating complement activation. α_1 antitrypsin possesses anti-inflammatory properties and regulates T- and B-lymphocytes. Transferrin plays a vital role in the innate immune system by activating macrophages. α_2 macroglobulin is an essential component of the innate immune system that regulates proteases and removes them from the bloodstream. The adsorption of these proteins to biomaterial surfaces may also direct the subsequent activation or inhibition of immune responses.

1.2 PEO: A gold standard low-fouling material

Surface modification with polyethylene oxide (PEO) has been known to inhibit nonspecific protein adsorption at the blood-biomaterial interface [4, 36, 37]. PEO is biocompatible and has shown exceptional oxidative stability in biological environments [38, 39]. It is superior to other protein-resistant polymers as it exhibits all four key characteristics of non-fouling materials [40]—

hydrophilicity, hydrogen bonding, electrical neutrality, and hydrogen bond acceptancy [41]. In addition, it is inherently flexible and provides configurational mobility, thus covering the protein adsorption sites on the surface [42]. Several mechanisms are proposed to explain PEO's protein-resistant behavior, however, the exact mechanism is still unknown.

1.2.1. Protein-resistance mechanisms of PEO

1.2.1.1 Steric repulsion theory

PEO's protein-repulsive behavior has been explained by the steric repulsion theory. As an effect of the inherent compressed nature of PEO layers, PEO chain conformational entropy decreases, PEO volume fraction and, thus, osmotic pressure increases, forcing water back into the polymer and protein, ultimately leading to reduced PEO-protein interactions [43, 44]. This is also called the osmotic pressure-entropy effect or steric stabilization effect and is thought to be dominant for high molecular weight polymers.

1.2.1.2 PEO-water interactions

It has been proposed that PEO's interactions with water play a crucial role in reducing protein adsorption, especially but not limited to PEO oligomers [45]. Hydration establishes an energy barrier that successfully hinders protein adsorption [46, 47]. It has been proposed that the first step of surface-protein interactions is the formation of a hydration layer at the biomaterial surface. Thus, instead of controlling other factors, monitoring proper surface-water interactions alone can reduce protein adsorption [45].

1.2.1.3 Effect of end groups

PEO can be modified with a number of end groups or distal groups including amines, cyanides, acrylate, methacrylate, carboxyl, methoxy, and hydroxy groups, out of which methoxy

and hydroxy-terminated PEO has been widely studied for protein adsorption [36, 37, 48, 49]. For oligoethylene oxide (OEO) modified with methoxy and hydroxy, the hydroxy-terminated polymers exhibited better protein resistance [50, 51]. It was found that the comparatively dense arrangement of methoxy groups tends to increase protein adsorption, whereas the more hydrophilic nature of hydroxy groups contributes to protein resistance [48]. The impact of the distal group becomes more significant when the chain density exceeds a critical threshold of 0.5 chain/nm^2 [48].

1.2.1.4 Van der Waals and electrostatic interactions

In addition to the inherent PEO properties, the surface-PEO-protein interactions significantly affect PEO-mediated protein resistance [52]. When the proteins have uncontrolled access to the surface, they adsorb faster by means of only diffusion, while the slower adsorption is the result of stronger protein-surface intermolecular interactions [48, 53]. Surface modification with PEO disrupts the water structures that support strong, long-range hydrophobic interactions and successfully screens the bare surface-mediated van der Waals interactions responsible for protein binding [54]. Despite the fact that tethered PEO film also exhibits van der Waals interactions, these interactions are generally weak compared to the film's high hydration level (~90%) [55]. The PEO modification of surfaces has been reported to eliminate the electrostatic forces induced by bare surfaces [56]. For OEO-alkanethiol surfaces, a distinctive ionic strength-dependent repulsive electrostatic force has been investigated that is active within the distance of a few tens of nanometers from the surface [57-59]. The inertness of OEO-modified surfaces has been found to be highly dependent on interfacial dipole moment orientation and resultant interfacial water structure [60, 61]. In a study on tri (ethylene glycol) modified gold surfaces, it

was found that the negative charges at the polymer solution interface readily give rise to electrostatic repulsive force [58, 59].

1.2.1.5 Chain density effects

Chain density effects play a crucial role in determining the protein resistance behavior of PEO [48]; however, there is limited research on precise variation in chain density and its significance in this context. For gold surfaces manipulated to achieve similar chain densities (0.5 chains/nm^2) but different chain lengths, the fibrinogen adsorption profile did not vary, suggesting that PEO chain density plays a more significant role in determining protein resistance than chain length [36]. Similarly, surfaces with constant PEO chain length (5000 MW) but slightly different chain densities exhibited considerable differences in protein adsorption profile, further suggesting that even smaller variations in chain density can affect the adsorption remarkably [37]. The increasing PEO chain density has significantly reduced the lysozyme and fibrinogen adsorption to PEO-modified surfaces [62].

The surface chain density of PEO directly influences the surface polymer conformation. Both chain density and PEO conformations can be manipulated by adjusting PEO solubility and chemisorption time [36]. PEO is soluble in water and, upon dissolution, obtains a conformation with multiple short helical chains interspersed with segments in a random coil configuration [63]. It has been suggested that when no external forces are applied, the polymer chains exhibit a spherical shape [55] with a radius (radius of gyration) termed as Flory radius (R_F), as explained below:

$$R_F = aN^{v} \qquad \text{Eq. 1.1}$$

Where *a* represents the characteristic monomer dimension (segment size), and its value is 2.78 Å for the ethylene oxide, *N* represents the degree of polymerization, and *v* the excluded volume exponent. The value of *v* is considered 0.5 for low solubility conditions or θ conditions. It can be seen here that R_F readily depends on *v*. The decrease in *v* leads to a lower water volume in the polymer, leading to less swelling of the polymer and eventually reducing Flory radius. With decreasing Flory radius, the volume occupied by individual polymer chains tethered on the surface in solution begins to overlap, causing increased lateral pressure that aligns polymer chains normal or perpendicular to the surface [64]. This leads to a decrease in graft spacing (*S*) or the distance between polymer attachment points and a subsequent increase in chain densities. With increasing chain density, polymer conformation changes from unperturbed random coil conformation (mushroom regime) to the extended PEO conformation (brush regime). Mushroom conformation occurs when the graft spacing (S) is more than twice the Flory radius ($2R_F$), whereas, the brush conformation is obtained when graft spacing is less than twice the Flory radius. The brush conformation, being associated with higher chain densities, provides maximum surface coverage and higher protein resistance and, thus, has been preferred in many studies involving PEO modification [36, 37, 48, 49]. The respective polymer conformations are illustrated in Figure 1.4.

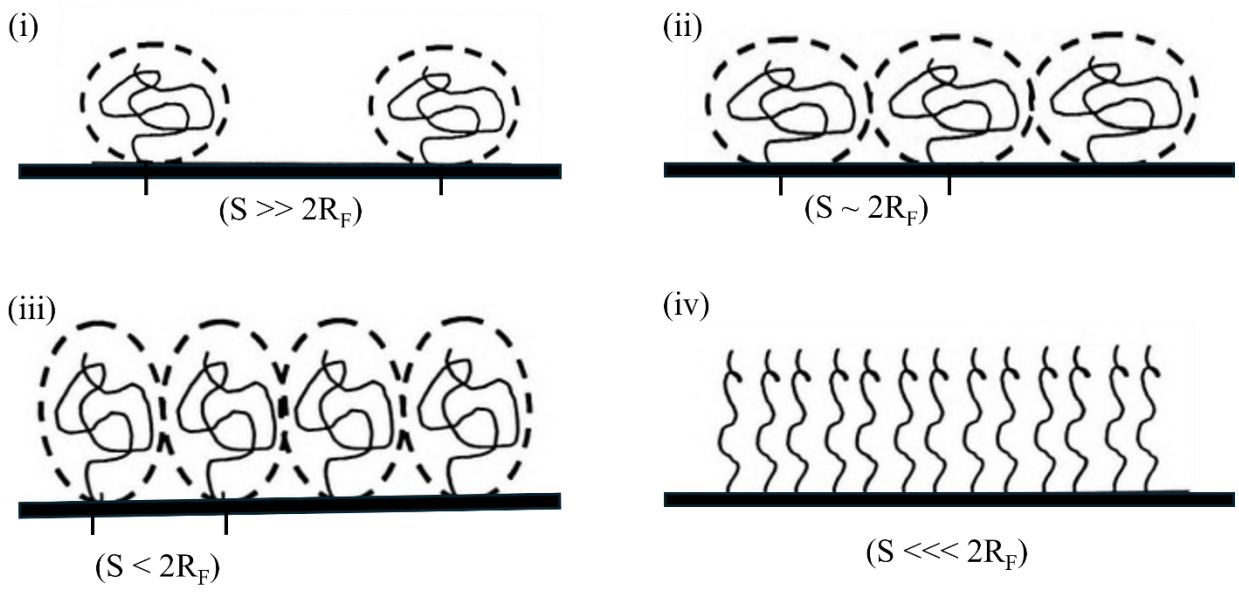

Figure 1.4. Representation of PEO film conformations. (i) Dilute nonoverlapping "mushrooms," (ii) Semi-dilute weakly overlapping "mushrooms," (iii) "Extended mushrooms" or dilute brush regime, and (iv) Highly extended chains or dense brush regime. Image reproduced from Unsworth et. al. [49] © Journal of Colloid and Interface Science, 2005.

The improved protein resistance at higher chain densities can also be explained by the hydration around the functional groups as chain density increases [48]. For methoxy-terminated PEO, the maximum in protein resistance was obtained at a chain density of 0.5 chains/nm² [36, 37]. This is the optimal value at which the distal chemistry or chain length does not have any effect on protein resistance [48]. However, the resistance dropped significantly when the chain density exceeded 0.5 chains/nm², possibly due to the dehydration of adsorbed polymer or the presence of hydrophobic contaminants at higher chain densities [37]. This suggests that the protein resistance varies directly with the chain densities, however, only until the optimal value is reached. The minimum chain densities needed to reduce fibrinogen adsorption effectively have been

reported to be $1.2x10^{-7}$, $4.2xl0^{-5}$ and $2.2xl0^{-5}$ chains/nm^2 for PEO of MW 3400, 10000, and 20000, respectively [65]. Chain densities have been reported to typically decrease with increasing PEO molecular weight under similar chemisorption conditions [48, 49]. All these pieces of evidence illustrate the importance of chain density in monitoring protein repulsion; however, a more comprehensive and in-depth understanding of the chain density effects is required.

1.3 Chronic kidney disease

1.3.1. Kidneys - the vital organs

Healthy kidneys perform several vital homeostatic functions, including waste removal, maintaining the metabolic acid-base balance, and fluid-electrolyte balance of the blood. In addition, they produce and regulate blood-pressure-controlling hormones, maintain calcium/potassium levels, and produce red blood cells [66]. However, the primary role of kidneys is to filter blood and produce urine with the aid of renal corpuscle and tubules, respectively referred to as filtration and reabsorption units. The renal corpuscles filter small molecules, such as water, ions, glucose, creatinine, and proteins under 90 kDa, whereas they prevent larger blood proteins, such as immunoglobulins, from passing through [66].

Kidney failure leads to the dysfunction of this filtration barrier and leads to chronic kidney disease (CKD). Statistically, a higher number (90%) of end-stage kidney diseases (ESKD) result from glomerular dysfunction [67]. The key issue is the kidney's limited regenerative capacity once damaged. Glomerular diseases typically progress slowly, with symptoms becoming visible only after a substantial loss of functional units [66]. The primary detrimental effect of kidney failure is a reduction in glomerular filtration rate (GFR), which dictates the severity of the disease, from

abnormal kidney function (GFR < 60 mL/min/1.73 m^2) to advanced CKD (GFR < 30 mL/min/1.73 m^2) to ESKD (GFR < 15 mL/ min/1.73 m^2) [68]. A reduced GFR leads to the accumulation of metabolites in the blood, commonly known as uremic toxins (UTXs) [69]. The UTXs are commonly removed using membrane-based filtration techniques such as hemodialysis. However, considering the wide range of UTX size and the cost and unfavorable health effects of hemodialysis, adsorption-based toxin removal strategies are also being developed [69, 70]. CKD is on the rise globally and is expected to rank as the 5th leading cause of premature mortality by 2040 [71]. Also, in the last 20 years, CKD's global prevalence has climbed by 30%, and the mortality rate across all ages has nearly doubled, affecting 700 million people worldwide [72, 73].

CKD highly influences host responses, including coagulation and immune responses [68]. Deteriorating kidney function leads to numerous hemostatic biochemical disorders, particularly affecting secondary hemostasis. This causes a significant increase in the blood concentration of fibrinogen, factors VII, VIII, and XII, activated protein C complex, homocysteine, and thrombin-antithrombin complex [68]. Reduced kidney function is also linked to higher levels of plasmin and antiplasmin [74, 75]. CKD patients have been reported to possess increasing bleeding risk due to platelet dysfunction [68]. In addition, CKD patients show abnormal adaptive immune responses that influence almost all immune system components, leading to CKD-associated immune dysfunctions [76].

1.3.2. Uremic toxins and their effects on protein adsorption

The presence of UTXs in the blood compartment readily alters the blood composition. UTXs that bind tightly to blood proteins, referred to as protein-bound uremic toxins (PBUTs), pose significant challenges for clearance from the blood using membrane-based techniques [77]. PBUTs, even after being cleared by hemodialysis, are released from the protein-bound phase in

plasma [78]. While not all UTXs are toxic, many of them, including uridine, guanidine, indoxyl sulfate (IS), hippuric acid, putrescine, p-cresol sulfate (PCS), and hypoxanthine, are identified for their harmful effects, and their concentrations have been documented in both normal and CKD conditions [79, 80].

Interactions between UTXs and plasma proteins have been observed to alter patterns of protein adsorption onto surfaces [1, 81]. However, there is limited research reported on this topic, and the direct mechanism remains unclear. It has been reported that metabolites and proteins mutually influence each other's adsorption to surfaces, as illustrated in Figure 1.5 [1]. UTXs present in the blood compartment have been documented to induce protein-folding events [82]. PBUTs, like IS and PCS, have been found to bind to human serum albumin *via* electrostatic and hydrophobic interactions and to change albumin's secondary and tertiary conformations significantly [77]. Several other toxins, including 3-carboxy-4-methyl-5-propyl-2-furanpropanoic acid (CMPF), hippuric acid, and indoleacetic acid have shown the strongest affinity to albumin [83]. The complex protein-metabolite interactions are dominant in regulating protein functions. These interactions sometimes lead to the formation of highly flexible and versatile molecular frameworks that behave distortedly in pathological conditions [84]. In a recent study on protein-metabolite interactions, the dataset for interactions between 3982 proteins and 74 small molecules was generated with the verification of 225 binding events [85]. In CKD patients, the excessive amount of blood urea leads to the carbamylation of certain proteins, for example, carbamylated alpha-lactalbumin (cLA), carbamylated fibrinogen (cFgn), and carbamylated human serum albumin (cHSA) which exhibit altered physiological responses [86, 87].

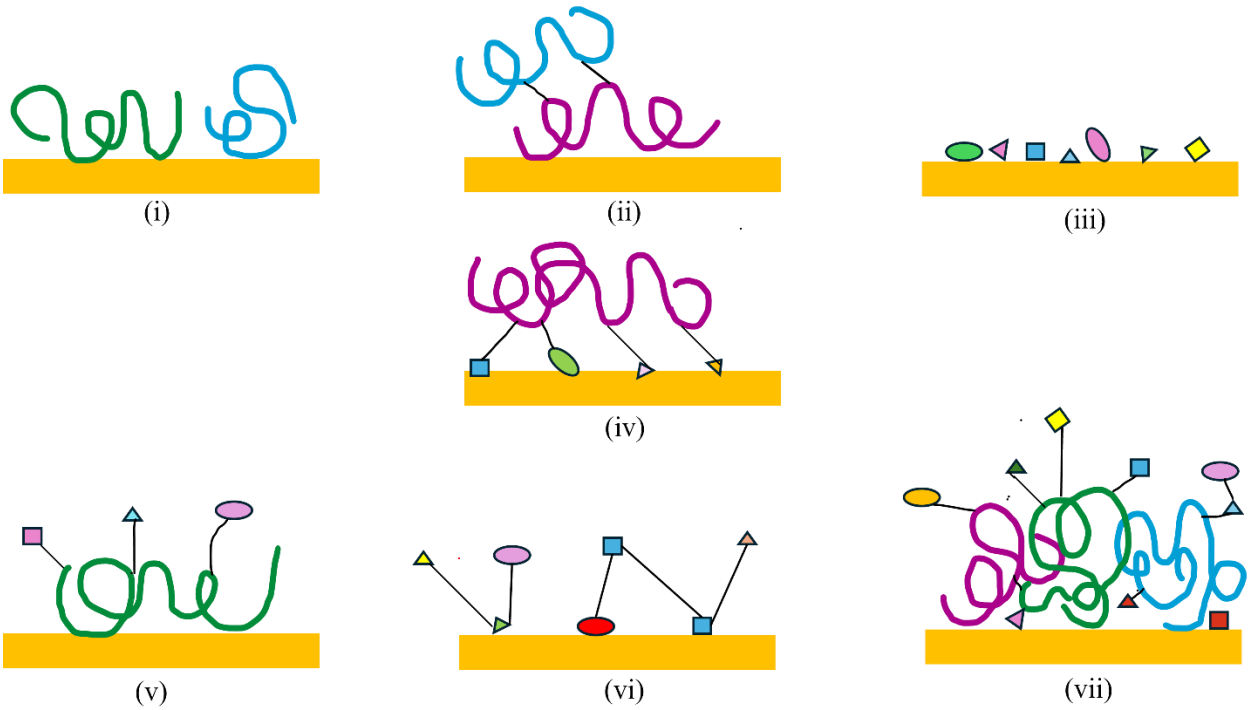

Figure 1.5. Adsorption of proteins and metabolites to surface. The interaction with surfaces is broken down into many steps: i) Direct adsorption of protein to surface; ii) Protein-induced adsorption of protein; iii) Direct adsorption of metabolites to surface; iv) Metabolite-induced adsorption of protein; v) Protein-induced adsorption of metabolites; vi) Metabolite induced adsorption of metabolites; and vii) Complex network of proteins and metabolites on surface. Image reproduced from Chetwynd et. al. [1] © Environmental Science Nano, 2020.

UTXs possess the ability to directly bind to surfaces, even low-fouling polymer films [69], and may alter their inhibitory effects on non-specific protein adsorption. For hemodialyzers and dialysis membranes designed to remove UTXs from the blood by adsorption-based strategies, the proteins and UTXs have been shown to compete with each other for adsorption [88]. A recent study by our group on 2-(methacryloyloxy)ethylphosphorylcholine-co-β-cyclodextrin (p(MPC-co-PMβCD)) films to adsorb toxins from a multicomponent toxin solution exhibited MPC's

natural low-fouling properties and β-CD's ability to bind with UTXs [69]. Studies have examined the direct adsorption of PBUTs, including IS, PCS, urea, and creatinine, onto various surfaces, such as polydopamine and amine-functionalized mesoporous silica [89, 90]. Tyrosine has been reported to cause structural changes to the low-fouling MA-41 heterogeneous electrodialysis membrane and deposit the tyrosine oxidation products on it [91]. The adsorption of asymmetric dimethylarginine has been successfully performed on poly (2-hydroxyethyl methacrylate-acrylic acid) nanoparticles, where the electrostatic interactions were the driving force [92]. The adsorption of spermine, putrescine, and spermidine has been investigated on sodium dodecyl sulfate surfaces as a function of their MW and structures [93]. In a study, less crystalline zirconium phosphate (ZrP) demonstrated superior adsorption of L-asparagine relative to fully crystalline ZrP, likely due to its more irregular surface structure [94]. When activated carbon was functionalized with sulfuric acid, the adsorption of urea and creatinine increased by 30 to 40 % [95]. Although the majority of these studies were aimed at developing adsorption-based UTX removal strategies, they illustrated the adsorption profile of UTXs on different surfaces, which is insightful in understanding UTX-surface interactions.

1.4 Research Motivation and Hypothesis

Protein adsorption at the biomaterial-blood interface can initiate a host response to materials, affecting host health and device function. Although PEO is regarded as the gold standard low-fouling material, the precise mechanism behind its protein resistance remains unclear due to the involvement of multiple factors. The PEO-mediated protein resistance is affected by surface chain density; however, only a few studies have successfully correlated protein adsorption with varying chain densities. In addition, all the studies on protein adsorption on PEO-modified surfaces have been conducted using healthy blood, overlooking the fact that blood composition is dynamic and disease-specific. When designing blood-contacting biomaterials for people with kidney dysfunction, it is crucial to consider the change in blood composition resulting from the accumulation of UTXs in their blood compartment. UTXs have been shown to form dynamic interactions with material surfaces, plasma proteins, and other UTXs. They have been proven to cause protein folding events and disrupt the secondary and tertiary structures of proteins. Their ability to bind directly to even low-fouling polymers such as PEO allows them to act as co-adsorbents and affect the adsorbed composition.

Therefore, we hypothesize UTXs affect protein adsorption to the PEO modified surfaces. Furthermore, we hypothesize that PEO chain density and chain end-group (OH *vs.* CH_3) have an effect on UTX-influenced protein adsorption at PEO-modified surfaces. These hypothesis were evaluated through forming end-tethered PEO-modified gold surfaces of varying chain densities using 750 and 800 MW PEOs with methoxy and hydroxy end-groups. These surfaces acted as versatile systems to adsorb proteins from plasma. The characterization of polymer films was performed using dynamic contact angle, ellipsometry, and X-ray photoelectron spectroscopy to determine fundamental polymer film properties, including hydrophilicity, thickness, and polymer

packing regimens. A series of 25 common UTXs with concentrations equivalent to those in HD patients were incorporated into plasma to mimic the unhealthy plasma, and protein adsorption experiments were performed. Adsorbed proteins were eluted, and the adsorption profiles of 20 plasma proteins were analyzed using standard SDS PAGE and immunoblotting techniques. Adsorbed protein band intensities allowed the comparison of surfaces for individual proteins' adsorption and to achieve the following key objectives:

i) The influence of uremic toxins on protein adsorption to methoxy-PEO-modified surfaces.

ii) The influence of uremic toxins on protein adsorption to hydroxy-PEO-modified surfaces.

iii) The influence of variable chain densities on protein adsorption to hydroxy-PEO-modified surfaces.

Chapter 2. Theory

2.1 Chemisorption of PEO

Chemisorption occurs when an atom or molecule binds to a surface through the overlap of one or more electron orbitals [96]. Chemical bonds are stronger than physical bonds, with the energy of adsorption reaching up to 800 kJ/mole [97]. It is irreversible and highly specific and thus occurs between selective adsorbent and adsorptive species. PEO is typically chemisorbed onto gold surfaces in order to achieve variable chain densities [36, 37, 48]. Although gold is typically considered inert, it binds strongly to sulfur-containing entities, such as thiols and disulfides [98]. Directly interacting the gold surface with thiolated (−SH) PEO solution is the most common method for coating gold surfaces with PEO monolayers. The three-fold hollow thiol binding sites are located between atoms of crystalline gold (Au(111)) surface at a distance of ~5 Å (due to the large size of the sulfur atom) [7]. The thiols bind to these sites when chemisorbed to face-centered cubic (fcc) gold (Au(111)). The 'Au–S' bond formed is a thiolate–Au+ coordination bond, with a homolytic bond strength of approximately 40 kcal/mol [99]. However, at elevated temperatures (400-500 K), they can desorb as thiol monomers (R-SH) by disrupting the S–Au bonds. The complete desorption of RS–Au complexes occurs at approximately 700 K [100].

The temperature at which PEO starts to precipitate in the solvent is referred to as the cloud point and is the key parameter in altering the film formed through the chemisorption of PEO [37]. Another important parameter is the PEO solubility, which is significantly influenced by solvent ionic strength, PEO concentration, and temperature. An increase in these variables leads to a progressive decrease in PEO solubility, eventually reaching the cloud point [37].

Higher chain densities can be achieved at the temperature near the cloud point where the polymer coils are contracted or comparatively smaller [36, 101, 102]. In contrast, under the chemisorption conditions further from the cloud point, the polymer coils are more expanded, giving lower chain densities [37]. The protein adsorption was substantially inhibited when chain densities were obtained by conducting the chemisorption near the cloud point and under low solubility conditions (also referred to as θ conditions), such as high ionic strength or high temperature [37]. The polymer solubility and chemisorption time can be varied near the cloud point to obtain the desired chain densities [36]. Increased chemisorption time often leads to higher chain densities. One of the major limitations of chemisorption is that it occurs only when the adsorbate is in direct contact with the surface and, therefore, forms only a single layer except for highly polar entities such as ammonia. It is highly dependent on temperature, and under inappropriate temperatures, the same surface can exhibit physisorption [97].

2.2 Advancing and receding contact angle

Contact angle measurements provide a simple and effective method to assess surface energies. The contact angle is primarily influenced by the properties of the solid and liquid, their interaction forces, and the characteristics of the three interfaces: liquid-vapor, vapor-solid, and liquid-solid (Figure 2.1). The advancing contact angle measures the droplet's angle at its leading edge on a dry surface, while the receding contact angle reflects the residual interaction forces when the liquid is removed from a wetted surface. Accurate measurement of the contact angle (θ) enables the calculation of surface tension using Young's equation as given below:

$$\Upsilon_{l-v}cos\theta = \Upsilon'_{s-v} - \Upsilon''_{l-s} \qquad \text{Eq. 2.1}$$

Here, θ represents the contact angle, while ϒ, ϒ', and ϒ'' denote the surface tensions of the liquid-vapor, vapor-solid, and liquid-solid interfaces, respectively.

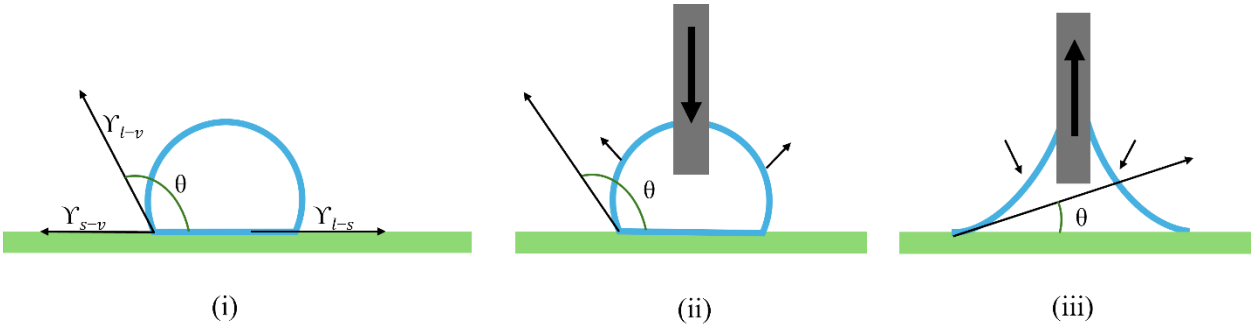

Figure 2.1. Contact angle measurements. (i) surface tensions of solid-air (Υ_{s-v}), liquid-vapor (Υ_{l-v}), and liquid-solid (Υ_{l-s}) interfaces, respectively. Illustration of (ii) advancing and (iii) receding contact angles.

However, this technique has some inherent limitations, such as optical limitations and inaccuracy in the measurement when the surface is too hydrophobic [103], chemically inhomogeneous, or rough [41]. Under such conditions, the Wenzel model and the Cassie-Baxter model can be applied. The Wenzel model characterizes rough and chemically homogenous surfaces where the droplet size is larger than the surface roughness. In this scenario, the droplet penetrates the surface structures, resulting in enhanced adhesive forces [41, 104]. In contrast, the Cassie-Baxter model applies to rough and chemically heterogeneous surfaces that are impenetrable to liquid droplets. Here, droplets rest on the surface's rough structures, trapping air underneath them [41, 104].

2.3 Spectroscopic ellipsometry

Ellipsometry is a highly sensitive, non-destructive optical reflectance technique with high precision in thin film metrology. It operates on the principle of variation in polarization of light reflected or transmitted from the sample surface and determines critical parameters, including optical constants (n, k) and film thickness [105].

Depending on the oscillation direction in an electric field, the light emission can be divided into p- and s-polarized. When two orthogonal light waves are in phase, the resulting light is linearly polarized, whereas when they are in arbitrary phase and amplitude, the resulting light is elliptically polarized (Figure 2.2). To perform the ellipsometry measurements, the amplitude (ψ) and phase change (Δ) for both p- and s- components in reflected or transmitted light are measured. For isotropic, non-absorbing layers, ellipsometry measurements are generally conducted with a single wavelength. However, for the characterization of non-isotropic complex structures, the samples are scanned with the wavelength across a broad spectrum.

Figure 2.3 schematically represents the operation principle of the ellipsometer. An unpolarized light is emitted by a light source that passes through a polarizer to become linearly polarized. The sample surface reflects the polarized light, transforms it into the elliptically polarized light, and then passes through a continuously rotating polarizer called the analyzer. The detector transforms the reflected light into an electronic signal and enables precise quantification of the reflected polarization. The data is compared to the known input polarization to quantify the amplitude and phase changes resulting from the sample's reflection.

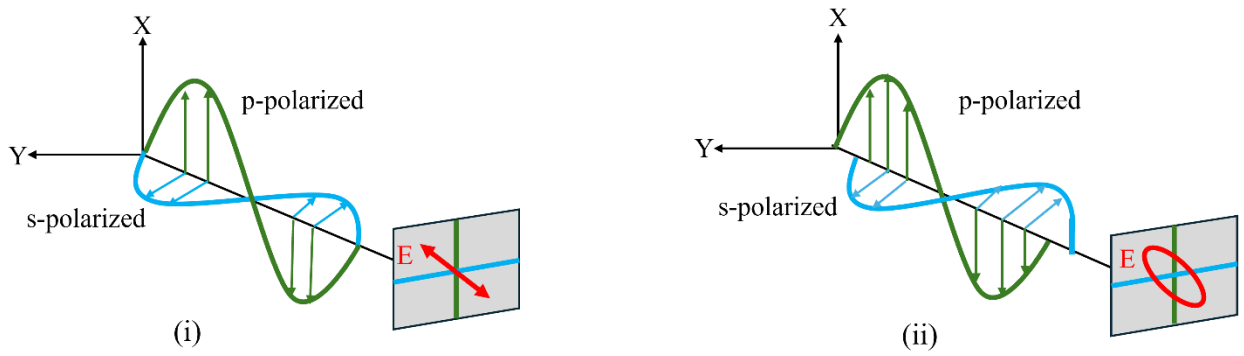

Figure 2.2. (i) Linear and (ii) Elliptical polarizations of light

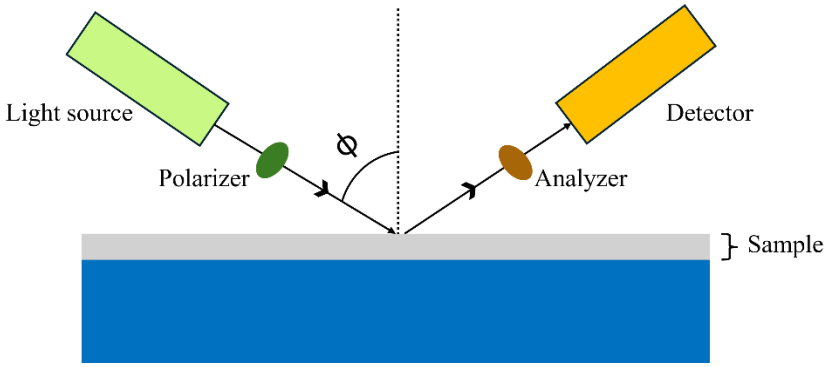

Figure 2.3. The ellipsometer operation principle. The polarized light is directed onto a sample, and the resulting change in polarization is analyzed. The angle of incidence, φ, can be adjusted as needed.

The amplitude ratio and phase difference between incident and reflected/transmitted light are represented by ψ and Δ, respectively. The parameter ψ is linked to the refractive index n, while Δ corresponds to the extinction coefficient k. Both ψ and Δ are derived from the ellipsometer using the Fresnel equations.

$$\rho = tan\psi e^{(i\Delta)} \quad \text{Eq. 2.2}$$

When the sample reflects light, Eq. 2.2 can be written as:

$$\rho \equiv tan\psi e^{(i\Delta)} \equiv \frac{r_p}{r_s} \quad \text{Eq. 2.3}$$

where r_p and r_s represent the amplitudes of reflection for p and s polarized light, respectively.

When the sample transmits the light, Eq. 2.2 can be written as:

$$\rho \equiv tan\psi e^{(i\Delta)} \equiv \frac{t_p}{t_s} \quad \text{Eq. 2.4}$$

where t_p and t_s represent transmission coefficients of p and s polarized light, respectively.

Challenges in precisely interpreting ellipsometry arise from factors such as the sample's surface characteristics, optical anisotropy, low spatial dispersion, and depolarization effects [106]. Recent developments, such as imaging ellipsometry, address better spatial resolution. The requirement for an optical data analysis model adds complexity to the analysis process, particularly for complex structures, and makes the process time-consuming [107]. Another limitation of this method is the need to assume a constant value for the film's mass density. This assumption has been evaluated by the previous study using neutron reflectometry, where the layer mass density for various systems was measured [49]. Based on this, a density value of 1.0 g/cm³ (for PEO) was adopted in the present study. Despite these limitations, spectroscopic ellipsometry provides high precision with value reaching up to 0.1 Å [108], making it a precise tool in the semiconductor manufacturing industries. Other advantages of spectroscopic ellipsometry include the non-invasive nature and high speed of measurements [108].

2.4 X-Ray photoelectron spectrometry

X-ray photoelectron spectroscopy (XPS) is a highly sensitive surface analysis technique to determine the atomic composition. XPS utilizes Einstein's photoelectric effect (Figure 2.4), where electrons are emitted from atoms in response to incoming electromagnetic radiation when the energy of incoming photons surpasses the binding energy of the material's electrons. The binding energies of the photoelectrons emitted from a surface sample serve as a "fingerprint" for identifying the elements present. Since atoms have various orbitals with distinct energy levels, the emission generates electrons with a range of binding energies leading to the XPS spectrum with peaks representing individual elements. The relationship between photon energy and binding energy can be expressed by the following equation [109, 110]:

$$E_{kinetic} = E_{photon} - E_{binding} \qquad \text{Eq. 2.5}$$

Where E_{photon} $(h\nu)$ represents the photon energy and E_b is the binding energy of the element. When the photon energy exceeds the binding energy, the excess energy is converted into kinetic energy, E_k.

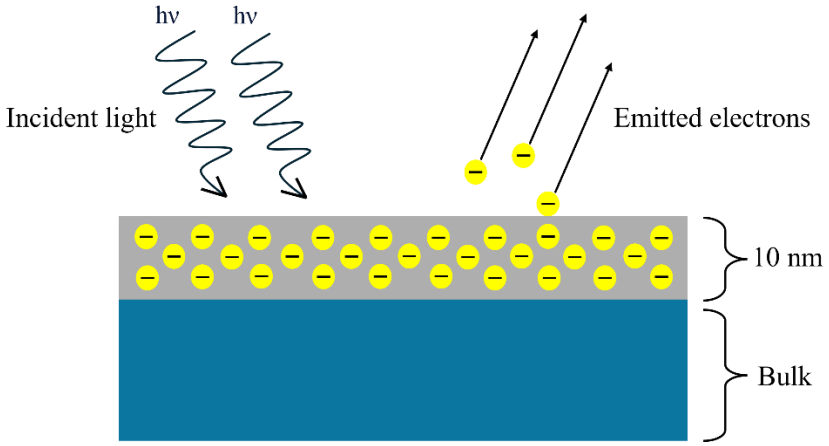

Figure 2.4. Photoelectric effect. Photons with energy $h\nu$ are incident to the surface, resulting in the emission of electrons with kinetic energy E_k.

A major limitation of XPS is that there is a maximum distance beyond which photoelectrons cannot escape from the surface, with 10 nm often regarded as the upper limit for soft surfaces [41, 111]. The high vacuum conditions are essential during measurements to obtain a steady signal and avoid contamination [41]. However, low-vacuum XPS technologies have been invented recently [112]. Similar to XPS, electron energy loss spectroscopy (EELS) [113] and energy-dispersive X-ray spectroscopy (EDX) [114] are two widely recognized analytical techniques for element detection. While EELS requires an electron beam to excite the electrons and is typically used for thin samples, EDX works with both electron beams and X-rays. X-ray absorption spectroscopy (XAS) [115] is another elemental determination technique that is more sensitive than XPS but needs higher energy to excite the electrons.

2.5 SDS PAGE and immunoblotting

Sodium dodecyl sulfate polyacrylamide gel electrophoresis (SDS PAGE) and immunoblotting (Figure 2.5), is an analytical technique used to separate, detect, and identify specific proteins within a complex mixture. The process involves separating proteins using gel electrophoresis and transferring them to a nitrocellulose or nylon membrane through an electroblotting technique. This is followed by a process called immunoblotting, where antibodies conjugated with probes, such as enzyme tags or chemiluminescent, fluorescent, or radioactive dyes, are used for the detection of individual proteins. The proteins are subsequently quantified using imaging software or techniques such as densitometry, depending on the chosen detection method [116, 117].

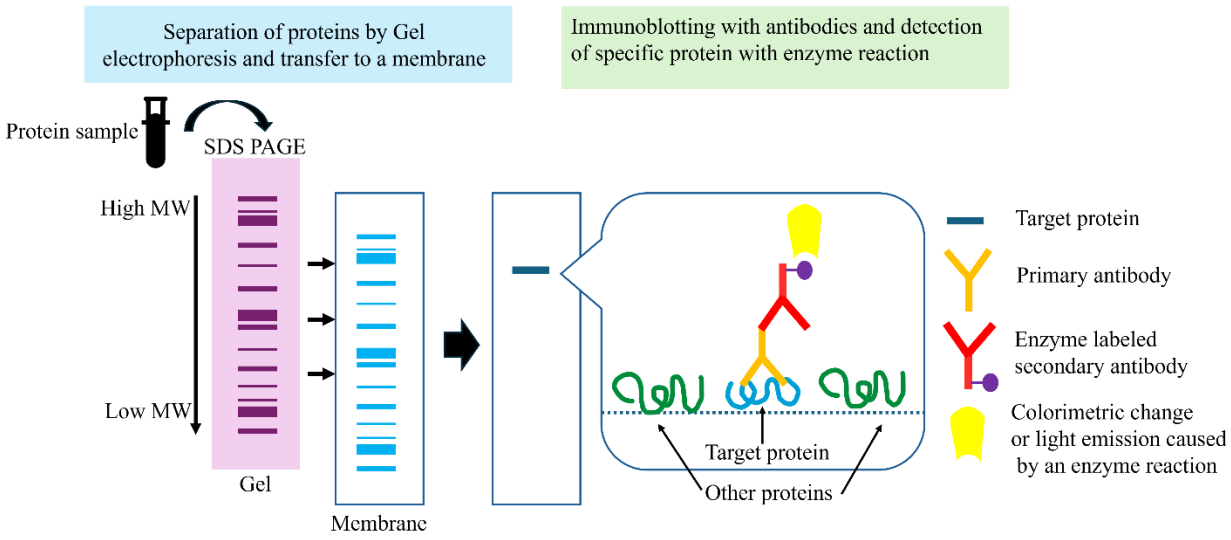

Figure 2.5. Principle of SDS PAGE and immunoblotting techniques.

2.5.1. Preparation of samples

Western blot samples are prepared by extracting proteins using specific cell lysis buffers or inhibitors that block protease and phosphatase activity. There are several extraction techniques, including sonication, homogenization, detergent lysis, and osmotic shock, depending on the sample type. It is crucial to have an equal concentration of proteins in each western blot sample. In the present study the protein sample consisted of plasma proteins eluted after adsorption to PEO-modified Au surfaces. Generally, the western blotting samples consist of three components: protein extract, cell lysis buffer, and sample (Laemmli) buffer. Sample buffer is specific to western blot sample preparation, with each reagent designed to facilitate SDS-PAGE [118, 119].

2.5.2. Polyacrylamide gel electrophoresis

The separation of proteins based on their molecular weight is achieved through SDS-PAGE. PAGE is a biochemical technique for separating proteins and nucleic acids depending on

their electrophoretic mobility in a gel. The addition of a strong anionic detergent (i.e., SDS) ensures that all denatured proteins acquire a uniform charge-to-mass ratio, making their movement through the gel dependent solely on molecular weight [119, 120]. Gel electrophoresis uses two types of gels: a stacking gel and a resolving or separating gel. The stacking gel, with larger pores, aligns proteins into a narrow band for entry into the resolving gel. The resolving gel, with smaller pores, facilitates the separation of proteins [119, 121]. Upon the application of proper voltage and current, higher MW proteins migrate more slowly toward the anode than lower MW proteins, as the pore size in the gel impedes their movement. Samples known as a protein ladder are loaded into their respective lanes alongside a molecular weight marker that provides standard molecular weight bands, which are used to determine the relative weights of proteins [122].

2.5.3. Transfer of gel contents

The electrophoretic transfer of gel contents, such as proteins onto a membrane is achieved in the process of blotting. Various blotting methods (wet, semi-dry, fast) and membrane types (polyvinylidene difluoride, nitrocellulose) are available, but the core principle of electrophoretic transfer remains consistent. Similar to electrophoresis, negatively charged samples move toward the anode. The transfer sandwich is arranged as filter paper, polyacrylamide gel, membrane, and then filter paper from cathode to anode [119, 123]. In a wet transfer system, fiber pads or sponges are placed on both sides of the sandwich assembly. A perpendicular current is applied to facilitate the movement of proteins from the gel onto the membrane.

2.5.4. Immuno-detection of proteins

The electrophoretic transfer immobilizes proteins on the membrane. The membranes are pre-incubated in a buffer to block non-specific binding sites before probing. Following this, primary antibodies are allowed to specifically bind to the target proteins, enabling their detection.

Subsequently, secondary antibodies, conjugated with an analytical marker, bind with the primary antibodies to facilitate the visualization of proteins [119, 124]. The analytical marker is a component tailored to the specific type of protein visualization technique. For example, autoradiography detects a radioactive isotope that is conjugated to a secondary antibody as a marker [125]. The frequently used detection method is chemiluminescence, which uses substrates that react with enzymes, typically horseradish peroxidase (HRP) or alkaline-phosphatase, conjugated to secondary antibody [119, 126]. In recent developments, fluorescence-based detection is becoming increasingly popular in detecting proteins, where secondary antibodies are linked to fluorophores, enabling detection directly without requiring substrate-based methods [119, 127].

There are some inherent limitations of the western blotting technique. Western blotting provides only semi-quantitative results and allows for approximate estimation rather than precise measurement of the protein's molecular weight [119, 128]. Off-target binding of the secondary antibody may lead to incorrect labeling of proteins [119, 129]. As the technique is highly sensitive, even minor deviations at any stage can significantly impact the accuracy of the results [130]. Another important fact is that antibody binding characteristics vary among different antibodies, allowing for discussion of their relative differences. However, comparing these differences can be challenging since band intensities may indicate lower levels of antibody binding. The adequate amount of HRP in the system partly addresses this issue.

2.6 Contribution to Research Articles

Different studies have performed protein adsorption experiments on various surfaces to understand protein adsorption profiles. In single protein adsorption experiments, the albumin adsorption to gold surfaces with polyurethane substrate was studied using a radioiodination technique [131]. The adsorption of proteins from pooled normal adult and infant plasma to polymethyl methacrylate, polyvinylchloride, and PEO-modified polyurethane surfaces has been studied using SDS-PAGE and immunoblotting techniques [132]. In a study by Unsworth et al., thiolated methoxy-PEO with molecular weights of 750, 2000, and 5000 were chemisorbed to a gold surface under various solubility conditions (to obtain variable chain densities), and protein adsorption profile from platelet-poor human plasma was reported [49]. A similar study has been performed to understand the role of chain densities in reducing fibrinogen and lysozyme adsorption to methoxy-PEO-modified Au surfaces [37]. The impact of PEO chain length (600, 750, 2000, and 5000 MW), chain density, and end groups (–OH, $–OCH_3$) on protein adsorption from plasma has been analyzed using immunoblotting and single-protein radiolabeling experiments [36], where the results supported the earlier finding [37] about the density of PEO chains being the crucial parameter in influencing the level of protein resistance. However, all these studies were based on the use of healthy blood, despite the provided evidence on UTX effects on adsorption surfaces and plasma proteins [1, 77]. The work presented here is the first attempt to understand the influence of UTXs on plasma protein adsorption to PEGylated surfaces. Chapter 3 of the present dissertation talks about the effect of both chain densities and UTXs on protein adsorption to methoxy-PEO-modified surfaces. Chapter 4 provides a similar understanding except for the use of hydroxy-PEO instead of methoxy.

Chapter 3. Effect of uremic toxins and methoxy-PEO chain density on plasma protein adsorption[1]

3.1 Introduction

Protein adsorption at the biomaterial-blood interface can influence the host response to materials, including coagulation, complement activation, and platelet activation [3, 4, 23, 36]. Polyethylene oxide (PEO) surface modification inhibits non-specific protein adsorption at the material interface [36]. Many features of this PEO film have been linked to the reduction in protein adsorption, including chain density, hydrophilicity, hydrogen bonding, and electrical neutrality [36, 40, 41]. It has been suggested that PEO-water interactions also influence the reduction of protein adsorption [45]. The role of PEO chain conformation on reduced protein adsorption has been studied for helical, linear, and loop conformations [133-135]. Changes in chain density can influence chain conformation, and a chain density of ~0.5 chains/nm^2 was shown to minimize fibrinogen adsorption to surfaces modified with end-tethered mPEO films [37, 101, 102, 136]. Although protein adsorption to PEO-modified surfaces has been extensively studied over the last 60+ years [36, 48, 137, 138], there is a disconnect between these research studies that use blood (i.e., plasma, serum, whole blood) from healthy donors who do not take medications and their application to unhealthy patients [139-141]. It is becoming apparent that blood composition is dynamic and highly dependent on the type of disease and its pathogenesis [70, 79]. It is well known that a reduction in glomerular filtration rate that occurs during kidney failure leads to the

[1] This chapter has been submitted as Aishwarya S Pawar[1], Ayda Ghahremanzadeh[2], Mehdi Ghaffari Sharaf[2], Larry D Unsworth[*], Effect of uremic toxins and methoxy-PEO chain density on plasma protein adsorption for publication in ACS Biomaterials Science & Engineering.

retention of uremic metabolites (i.e., uremic toxins) in the blood compartment [69]. This work is a first step in understanding the dynamics and specificity of the interaction between blood-borne uremic toxins (UTXs) and classic PEO-modified surfaces, which is necessary to advance both low-fouling surface science and, ultimately, a personalized medicine approach for these patients.

Kidney failure leads to the retention of UTXs in the blood, a fraction of which have been quantified (Table 3.1). Although the toxicity of all retained UTXs has not been established, several are toxic and cause systemic complications, like indoxyl sulfate, p-cresyl sulfate, urea, creatinine, and hippuric acid [89, 90, 142]. It is unknown how the complex buildup of metabolites in the blood compartment affects the adsorption of proteins to surfaces. It has been observed that some metabolites trigger protein folding events [82], and their interactions with proteins alter the protein adsorption mode on surfaces [1]. Selected UTXs, mostly protein-bound, have been studied for adsorption to surfaces of different types but usually from the point of view of adsorbing the uremic toxin to clear it from blood rather than their effect on protein-surface interactions [89, 90]. For example, polydopamine coatings on diatomaceous earth and poly-vinyl-pyrrolidone-co-styrene enhanced the adsorption and retention of indoxyl sulfate and p-cresyl sulfate and PDA-coated materials improved entrapment and retention of the UTXs from patients' serum [89]. A zeolite composite nanofiber mesh was synthesized to adsorb indoxyl sulfate from a single-component aqueous solution [142]. Work recently published by our group is the only one that investigated the adsorption profile of UTXs from a multicomponent toxin solution to poly 2-(methacryloyloxy)ethylphosphorylcholine-co-β-cyclodextrin (p(MPC-co-PMβCD)) films, leveraging MPC's inherent low-fouling characteristics and β-CD's capability to bind with UTXs [69]. The biocompatibility and protein adsorption experiments were carried out for p(PMβCD-co-MPC) magnetic nanoparticles – a novel material for toxin removal from blood [23]. It suggested

that the introduction of UTXs caused the modified MNPs to delay the formation of clotting [23]. However, this previous work primarily focused on synthesizing more efficient adsorbents, while the ultimate goal of our current study is to understand the direct effect of plasma-borne UTXs on the adsorption of proteins to PEO-modified surfaces.

For this study, we hypothesize that plasma-laden UTXs in the average concentration found for end stage kidney disease (ESKD) patients alter the adsorption of plasma proteins to low-fouling films composed of PEO. To this end, surfaces were modified with methoxy-terminated polyethylene oxide (mPEO, 750 MW) with variable chain densities. Plasma was doped to contain 25 UTXs with a final concentration similar to that found in HD patients (Table 3.1). Fundamental properties like hydrophilicity, elemental composition, and polymer chain densities were determined for the PEO films. Adsorbed proteins were eluted and analyzed using immunoblotting techniques. Differences in chain densities and the presence of UTXs led to significant changes in individual protein band intensities. These data suggest that the presence of UTXs significantly alters the composition of the adsorbed protein layer. Further work is necessary to understand the role of UTXs on low-fouling surfaces to develop a personalized dialysis approach.

Table 3.1. Uremic toxin concentrations in ESKD patients undergoing hemodialysis therapy.

Uremic toxins	Experimental concentration (mg/L)	Patient concentration (Ave ± 1 SD, mg/L)	Ref
4-Ethylphenyl sulfate	0.25	0.242 ± 0.044	[143]
Indole acetic acid	2.03	2.03 ± 0.38	[79]
L-Tyrosine	54.35	54.35 ± 16.3	[144]
Asymmetric dimethylarginine	0.38	0.385 ± 0.2884	[79]
Hypoxanthine	2	2.0 ± 1.6	[80]
Spermidine	0.096	0.097 ± 0.045	[79]
Argininic acid	0.075	0.08 ± 0.056	[80]
3-Deoxyglucosone	1.7	1.7 ± 1.0	[80]
Homocysteine	8.1	8.1 ± 1.6	[80]
L-Asparagine	7.16	7.13 ± 3.7	[145]
Pyruvic acid	11.7	5~11.7 ± 8.6	[146]
Trimethylamine N-oxide	7.5	7.49 ± 2.39	[147]
Creatinine	136.4	136.0 ± 46.0	[80]
Hippuric acid	237	247.0 ± 112	[80]
Uric acid	83	83 ± 13	[148]
Xanthosine	96.6	96.6 ± 62.9	[149]
Putrescine	0.001	0.00942 ± 0.00759	[79]
Uridine	9.8	9.8 ± 11.4	[80]
Dimethyl glycine	0.59	0.5768	[80]
Guanidinopropionic acid	0.288	0.288 ± 0.0183	[80]
p-Hydroxyhippuric acid	4.25	4.43 ± 2.79	[150]
Phenylalanine	9.25	8.92 ± 1.81	[151]
Indoxyl glucuronide	2.5	2.5 ± 0.3	[79]
Indoxyl sulfate	53	53.0 ± 91.5	[80]
Spermine	0.002	0.018 ± 0.0162	[80]

3.2 Materials and methods

Chemicals used for Experiment: Methoxy-terminated polyethylene oxide (750 MW) was obtained from Biopharma PEG Scientific Inc (Watertown, MA, USA). Platelet-poor human plasma was acquired through the Blood4Research initiative from Canadian Blood Services. HPLC-graded water, PBS tablets (pH 7.4), tris base, and 40% acrylamide were sourced from Fisher Scientific. Polyvinylidene fluoride (PVDF) membrane and sodium dodecyl sulfate (SDS)

were obtained from Bio-Rad, Hercules, CA, USA. The TMB-stabilized substrate was acquired from Promega, Madison, WI, USA. Tween 20, TEMED, β-mercaptoethanol, and glycine were procured through Sigma Aldrich, nonfat dry milk (Carnation dry milk), colloidal gold solution, and ladder solution were obtained from Bio-Rad labs, USA. All chemicals were used as received without further purification. See Table A1 in the Appendix A for the complete list of antibodies.

Chemicals used to prepare UTX solution: 4-Ethylphenyl sulfate (98%) was acquired from Apexbio (Houston, USA), and 4-Hydroxyhippuric acid (≥98%) from Cayman Chemical. A substantial collection of chemicals was obtained by Sigma Aldrich, including Phenylalanine (≥98%), Uridine (≥99%), Trimethylamine N-oxide (≥95%), Uric acid (≥99%), homocysteine (≥98%), Indoxyl sulfate, Indoxyl glucuronide (≥98%), Xanthosine, putrescine (≥98%) Guanidinopropionic acid (≥97.5%), Spermine (≥97%), Creatinine (≥98%), Spermidine (≥99%), L-Tyrosine (≥99%), Asymmetric dimethylarginine (≥98%), Pyruvic acid (≥98%), hypoxanthine (≥99%), 3-Deoxyglucosone (≥75%), Dimethylglycine (≥99%), Hippuric acid (≥98%), 3-Indoleacetic acid (≥98%), and L-Aspargine (≥98%). L-argininic acid was acquired from Toronto Research Chemicals (Ontario, Canada).

3.2.1. Chemisorption of PEO

Silicon wafers from Thin Film Technology, Buellton, CA, were treated to remove the oxide layer, coated with 500 Å chromium (for adhesion) and 2000 Å Au, and then diced into 0.5 x 0.5 cm chips. The chips underwent cleaning in a solution of hydrogen peroxide, ammonium hydroxide, and water (in a ratio of 1:1:5) at 80 °C for 5 minutes to eliminate carbonaceous contamination. Following this, they were rinsed in HPLC-graded Milli-Q water and then placed into wells of a 96-well microtitre plate filled with the same. The plates were kept for equilibration at 58 ºC for 30 minutes.

The chemisorption solution conditions were adjusted to achieve three different PEO chain densities. A 5-mM solution of methoxy (-OCH_3) terminated, end-thiolated PEO (750 MW) was prepared in PBS-K_2SO_4 buffer (0.1 M PBS, 0.6 M K_2SO_4, pH 7.4) of ionic strength 3.1 M, using previously published methods [37, 49, 152], and filled in wells of 96-well microtiter plates. To ensure a consistent temperature, the plates were equilibrated under the same conditions as the chips, and then the chips were transferred into the PEO-thiol solution using forceps. The chemisorption was performed following low solubility conditions (typically θ conditions) of the polymer at 58 ºC. The variable chain densities were achieved by varying the time (10 min, 30 min, and 4 hrs) near the cloud point, as mentioned previously [101, 102]. After chemisorption, the wafers were rinsed extensively with HPLC-graded Milli-Q water to remove loosely adsorbed polymer.

3.2.2. Characterizations of PEO films

3.2.2.1 Contact angle measurements

The dynamic contact angles of mPEO films were characterized using the Attension Theta Lite Optical Tensiometer (Nanoscience Instruments, USA). Advancing and receding water contact angles were measured by forming water drops on the surfaces, with a volume not exceeding 2 µL and an advancing/receding rate of 0.2 µL/s. The drops were allowed to advance and recede on the chips for 40 seconds while the values were recorded. The statistical difference between values was evaluated using an unpaired Student's *t*-test.

3.2.2.2 Measurement of polymer chain densities

The thicknesses of dried mPEO films, chemisorbed to surfaces, were evaluated using a 370 – 1000 nm wavelength, variable-angle M-2000V spectroscopic ellipsometer. The CompleteEASE, J.A. Woollam software was used to fit the obtained data and to determine the extinction coefficient

(k) and refractive index (n). To do this, a B-spline model was applied with node spacing set at 0.1 eV and Au metal as a base. The Au optical constants were used as substrates for mPEO films, and a Cauchy model was applied to reveal the thickness of PEO. As PEO is a transparent organic compound, the lowest Cauchy parameters were used as A (1.45) and B (0.01). The respective chain densities were calculated using dry film properties as given in the following equation.

$$L = \left(\frac{M}{\rho_{dry} d N_A}\right)^{1/2} \quad \text{Eq. 3.1}$$

In this equation, the mean distance between polymer attachment points on the surface is denoted by L. M represents the molecular weight of PEO, ρ_{dry} is the dry PEO layer density (initially assumed to be 1.0 g/cm³), d indicates the mean layer thickness of PEO (as obtained from ellipsometry), and N_A refers to Avogadro's number. The final polymer chain density can subsequently be evaluated as L^{-2}. An unpaired Student's *t*-test was performed for some values to analyze their statistical difference.

3.2.2.3 Elemental composition of PEO films

Kratos Axis (Ultra) spectrometer (Kratos Analytical Ltd, UK), with monochromatized Al Kα (hυ = 1486.71 eV), was used to generate X-ray photoelectron spectroscopy (XPS) spectra at room temperature. The binding energy (84.0 eV) of Au 4f7/2 with reference to the Fermi energy level was used to calibrate the spectrometer. The atomic compositions (%) were determined by analyzing a low-resolution survey spectrum (binding energies from 0 to 1100 eV), which was collected at the analyzer (pass energy = 160 eV). The spectral fitting was performed using CasaXPS (Casa Software Ltd., Japan), and elements were quantified (%).

3.2.3. Protein adsorption from plasma

Platelet poor plasma collected from healthy human donors was obtained from Canadian Blood Services, aliquoted, and stored at -80 ^{o}C degrees. Human platelet poor plasma was used in accordance with approved research ethics board approvals: Canadian Blood Services 2022-21, and University of Alberta Pro00002363 and Pro00116764. Protein adsorption from plasma was accomplished by incubating surfaces (four for each time point) in undiluted plasma under static conditions at room temperature for 3 hrs [36]. To avoid any potential overlap of samples, the non-adherent 96 well plates were used for plasma incubation. Following incubation, the samples underwent three rinses (each lasting 10 min) in PBS buffer to remove loosely adsorbed protein.

To simulate the blood composition of CKD patients, the collection of 25 UTXs was incorporated into the plasma before incubation. The concentrations of UTXs were maintained to mimic their levels in HD patients. The UTX solution was pre-prepared, aliquoted, and stored at -80 ^{o}C, then subjected to freeze-drying and subsequent storage at -20 ^{o}C before utilization. To each UTX aliquot, 1 mL of plasma was added, mixed, and left at room temperature for 30 min to facilitate complete dissolution and well-mixed UTX-plasma solution.

3.2.4. SDS-PAGE and immunoblotting

Sodium dodecyl sulfate polyacrylamide gel electrophoresis (SDS-PAGE) and immunoblotting were used to evaluate and identify individual proteins eluted from those adsorbed to PEO-modified surfaces [36]. Proteins were eluted using a 2% aqueous sodium dodecyl sulfate (SDS) soak overnight at room temperature. Each system was sonicated for two minutes before and after the elution to obtain the best possible collection of adsorbed proteins.

Prior to SDS-PAGE, eluted samples were treated with a denaturing sample buffer containing SDS and 0.5 M β-mercaptoethanol, followed by heating at 95 °C for 5 min. All samples were run together on an SDS-PAGE gel (12% separating, 4% stacking gel) and transferred electrophoretically to 0.2 μm-pore size immobilon polyvinylidene fluoride (PVDF) membranes (Millipore, Bedford, MA). The adsorption surface area, the volume of SDS buffer used for elution, and the volume of eluate loaded on each gel were kept consistent in all experiments. The blot membrane was cut into strips and exposed to primary antibodies (1:1000 diluted) for specific proteins at room temperature. Alkaline phosphatase-conjugated affinity-purified secondary antibodies (1:1000 diluted) were used to target primary antibodies at the same experimental conditions. The strips were subsequently exposed to a TMB-stabilized HRP conjugate solution (a chromogenic substrate) to visualize the individual proteins. Separately, the ladder strips of membrane blot were stained with colloidal gold solution to visualize the protein bands. Further, the strips were dried, reassembled, and scanned for quantification of band intensities using ImageJ 1.53e, USA. The intensity of immunoblot bands for all surfaces was analyzed using a 12-step grayscale system, with '0' indicating no discernible band and '12' representing the highest band intensity. Across all systems studied, uniform protein loading volume and consistent color development time were maintained to facilitate the comparison of band intensities between different systems.

3.3 Result and discussion

3.3.1. Advancing and receding contact angles

Contact angles were collected to prove PEO modification of the Au surface (Table 3.2). Advancing and receding contact angles decreased significantly ($p<0.0001$) for all mPEO modified surfaces with respect to Au controls (Table 3.2), confirming mPEO modification. It was apparent

from the data that both advancing and receding contact angles decreased with increasing chemisorption time. However, the values for 10 and 30 min mPEO systems were not statistically different (p_{adv} = 0.14, p_{rec} = 0.82). The advancing contact angle for the 10 min mPEO system (46 ± 2 °) was similar to previous findings (46 ± 1 °) [49] under low solubility conditions. The advancing and receding contact angles for 30 min (43.54 ± 0.18 °, 38.0 ± 0.9 °) and 4 hr (39.9 ± 1.1 °, 33.1 ± 0.4 °) modified systems were statistically significant (p_{adv} = 0.0051, p_{rec} = 0.0012), and slightly higher than those previously obtained under low solubility conditions [49].

Table 3.2. Advancing and receding contact angles for mPEO-modified Au-surfaces. Data are mean ± SD (n ≥ 3).

Surface	Advancing (°)	Receding (°)
Unmodified Au	81.6 ± 1.2	74.3 ± 2.4
10 min mPEO modified	46 ± 2	38.2 ± 1.3
30 min mPEO modified	43.5 ± 0.2	38.0 ± 0.9
4 hr mPEO modified	39.9 ± 1.1	33.1 ± 0.4

3.3.2. PEO chain density

mPEO chain density after 10 min, 30 min, and 4 hr incubations were 0.52 ± 0.06, 0.50 ± 0.12, and 0.81 ± 0.03 chains/nm^2, respectively. These were higher than that expected for monolayers of unperturbed random coils (mushroom conformation) [49], but less than the reported highest value of 5.8 chains/nm^2 for fully extended polymer chains [49, 153], suggesting that mPEO layers were in the brush regime for all surfaces. There was a significant ($p<0.0001$) increase in chain densities from 10 min (0.52 ± 0.06) to 4 hr (0.81 ± 0.03). The chain density after 30 min of incubation was not statistically different from the 10 min surfaces (confirmed by student *t*-test, p = 0.78). The chain density value obtained for the 4 hr incubation system was considerably higher

than the previously reported value (0.63 ± 0.13 chains/nm^2) [49], but different chemisorption conditions were used that may lead to a higher chain density.

3.3.3. Elemental composition

The atomic compositions derived from low-resolution XPS data (Table 3.3) indicate that unmodified Au contained 27.5% carbon and 10.3% oxygen, likely reflecting the presence of atmospheric carbonaceous contamination [154]. The remarkable reduction in Au content, alongside the substantial increase in carbon and oxygen levels from unmodified to modified samples [4] indicated the successful deposition of PEO on the surfaces [41]. As chain density increased on PEO-modified surfaces, the reduction in Au content and the increase in carbon and oxygen levels [49] confirmed a more extensive PEO deposition with increasing chain density. As sulfur is not the component on unmodified Au surfaces, it acts as a unique identifier for adsorbed thiolated PEO. Its presence on PEO-modified surfaces further signified the successful PEO modification. The obtained values for the C:O ratio resembled the theoretical value of 1.9 for mPEO.

Table 3.3. Atomic compositions (%) of PEO films from low-resolution XPS data. Data are mean ±SD, n = 3.

Surface	Element composition (%)				
	Au 4f (83 eV)	O 1s (532 eV)	C 1s (285 eV)	S 2p (165 eV)	C:O
Bare Au	62.3 ± 4.5	10.3 ± 0.9	27.5 ± 4.2	0	2.7 ± 0.4
10 min mPEO	53.8 ± 1.3	15.8 ± 1.2	28.5 ± 0.6	2 ± 0.2	1.8 ± 0.1
30 min mPEO	49.9 ± 1.6	17.3 ± 0.8	30.7 ± 1.3	2.1 ± 0.2	1.8 ± 0.1
4 hr mPEO	47.4 ± 1.1	19.5 ± 1	31.5 ± 1	1.6 ± 0.5	1.6 ± 0.1

3.3.4. Adsorbed protein analysis

Proteins eluted after plasma incubation were analyzed using immunoblot techniques to assess the impact of variable mPEO chain densities and UTXs on plasma protein adsorption. Loading equal volumes of eluents onto each gel enabled a comparative analysis of the relative band intensity of each protein across various surfaces. It was not possible to determine the total adsorbed amount of protein to these surfaces using the Pierce™ BCA protein assay with a lower detection limit of 20 μg/mL. The major proteins identified involved albumin, complement C3, IgG, fibrinogen, and factor XI on all surfaces (Table 3.4 and Table 3.5). In addition, trace amounts of prothrombin, α_1 antitrypsin, transferrin, and vitronectin were obtained in selected samples, although in low quantities.

Albumin (66 kDa) constitutes nearly 50% of the plasma protein pool, and is known to adsorb to a variety of biomaterial surfaces [155]. Previous studies have shown high amounts of albumin adsorbed onto both bare and PEO-coated Au surfaces, with PEO coatings sometimes increasing the bound amount of albumin [36]. In both normal and UTX plasma, albumin was found in high levels adsorbed to PEO-coated surfaces. In normal plasma, there was an increasing trend in albumin adsorption from bare surfaces (scale 6) to higher PEO chain densities, reaching a very high adsorption level (scale 10) in the mPEO 4 hr system; perhaps due to the increased presence of the methoxy end group at the material interface. In UTX plasma, most surfaces exhibited a substantial increase in albumin adsorption compared to the normal plasma and the maximum band intensity of 12 was observed for the mPEO 30 min system, decreasing to 8 for the 4 hr incubation systems.

Table 3.4. Relative intensities for western blots of human plasma proteins adsorbed to surfaces with different chain densities, ranging from 0 (no detectable intensity) to 12 (maximum intensity). Lower values indicate less eluted protein from the surface.

Plasma Proteins			Fragment size (kDa)	Au control	PEO 10 min	PEO 30 min	PEO 4 hr
	Albumin		66	6	8	8	10
Immune response-related	C3:	Whole C3	187	0	0	0	0
		α chain	115	0	0	0	0
		β chain	70	1	7	4	6
		Activation fragment	42	0	6	3	2
	IgG:	Heavy chain	55	0	1	1	1
		Light chain	27	1	2	1	3
	Transferrin		77	0	2	0	0
	Vitronectin		54	0	0	0	2
	α_1 antitrypsin		54	0	1	0	0
	α_2 macroglobulin		163	0	0	0	0
Coagulation related	Fibrinogen:	α chain	68	1	1	4	3
		β chain	56	1	2	5	2
		γ chain	48	1	1	2	1
		Cleavage fragments	<48	0	0	0	0
	Fibronectin		259	0	0	0	0
	Prothrombin		72	0	1	0	0
	Antithrombin		53	0	0	0	0
	Factor XII		80	0	0	0	0
	Factor XI		70	7	4	3	9
	Kininogen (heavy)		120	0	0	0	0
	Protein C		62	0	0	0	0
	Protein S		75	0	0	0	0
	Prekallikrein		85	0	0	0	0
	Plasminogen		91	0	0	0	0

0
1 to 3
4 to 5
6 to 7
8 to 9
10 to 11
12

Table 3.5. Relative intensities for western blots of human plasma proteins adsorbed to surfaces with different chain densities in the presence of UTXs. While 0 detects no proteins adsorbed, 12 indicates the maximum intensity. Lower values indicate less eluted protein from the surface.

Plasma Proteins			Fragment size (kDa)	UTX-Au control	UTX-PEO 10 min	UTX-PEO 30 min	UTX-PEO 4 hr	
	Albumin		66	9	11	12	8	0
								1 to 3
Immune response-related	C3	Whole C3	187	1	1	0	0	4 to 5
		α chain	115	0	1	0	0	6 to 7
		β chain	70	2	9	7	9	8 to 9
		Activation fragment	42	0	7	5	8	10 to 11
	IgG	Heavy chain	55	1	2	2	1	12
		Light chain	27	2	5	3	4	
	Transferrin		77	1	1	1	1	
	Vitronectin		54	0	0	0	0	
	α_1 antitrypsin		54	1	1	1	0	
	α_2 macroglobulin		163	0	0	0	0	
Coagulation related	Fibrinogen	α chain	68	5	3	8	1	
		β chain	56	5	1	2	1	
		γ chain	48	3	1	1	1	
		Cleavage fragments	<48	0	0	0	0	
	Fibronectin		259	0	0	0	0	
	Prothrombin		72	0	0	1	1	
	Antithrombin		53	0	0	0	0	
	Factor XII		80	0	0	0	0	
	Factor XI		70	7	2	3	4	
	Kininogen (heavy)		120	0	0	0	0	
	Protein C		62	0	0	0	0	
	Protein S		75	0	0	0	0	
	Prekallikrein		85	0	0	0	0	
	Plasminogen		91	1	0	0	0	

3.3.4.1 Clot associated proteins

Fibrinogen bands for the α, β, and γ chains show at 68, 56, and 48 kDa, respectively. Bands below 48 kDa indicate fibrinogen cleavage due to activation of the fibrinolytic system. All samples, including the Au control, demonstrated very low to intermediate fibrinogen band intensities. Significantly, none of the samples exhibit detectable cleavage bands of fibrinogen, suggesting that although fibrinogen adhered to all modified surfaces, its cleavage was minimal. The responses for α and β chains remarkably increased for Au control upon UTX addition. While the introduction of toxins resulted in a notable elevation of the α chain for the UTX-PEO 30 min sample, the intensity for the β chain of the same surface showed a decline. A huge downturn in the intensity values of α and β chains from UTX-Au control to UTX-PEO 10 min suggested that the anti-fouling effect of PEO was apparent in the presence of UTX. Other surfaces showed no significant change with UTX addition. Studies on single protein adsorption indicate that increasing the PEO chain density on Au surfaces enhanced resistance to fibrinogen adsorption [37]. This has been further confirmed *via* chemisorbed PEO layers with various chain densities on Au surfaces interacting with normal plasma, where among the different PEO-coated surfaces, those formed from solutions near the cloud point adsorbed the least amount of fibrinogen from plasma [36].

The coagulation contact pathway involves three serine proteinases: prekallikrein (85 kDa), coagulation factors XI (70 kDa) and XII (80 kDa), and the non-enzymatic cofactor high-molecular-weight kininogen (120 kDa) [23, 156]. These four proteins can interact with blood-contacting surfaces, initiating a cascade that yields activated factor XI, which perpetuates clotting, ultimately leading to fibrin formation [36]. In this study, surfaces exhibited variable levels of factor XI, ranging from low to moderately high. While the addition of UTXs did not notably affect surface adsorption, a significant decrease in band intensity of factor XI was observed for the highest chain

density sample. The prekallikrein, coagulation factor XII, and high molecular weight kininogen were absent across all samples, even after adding UTXs. This suggests that the activation of coagulation through these contact phase proteins was unlikely, irrespective of UTX presence. These findings are consistent with previous studies where Au surfaces coated with PEO monolayers of varying molecular weights exhibited either no detectable bands or weak bands for most contact phase proteins [36]. PEO coatings have been demonstrated to decrease the surface adsorption of high-molecular-weight kininogen compared to bare Au surfaces [36].

Prothrombin (72 kDa) is an inert precursor to thrombin. In normal plasma, prothrombin was not detected to be adsorbed to any of the surfaces, except for a faint band in the PEO 10 min system. In UTX plasma, no notable change in surface adsorption of this protein was observed. This indicates that neither PEO chain densities nor the addition of UTXs significantly affected its presence. Antithrombin, a potent inhibitor of thrombin-mediated coagulation, was entirely absent from all eluted protein samples. Plasminogen, critical to fibrinolysis, exhibited identical behavior. Studies have shown that PEO-grafted polyurethane surfaces adsorb less prothrombin and plasminogen than polyvinyl chloride and polymethyl methacrylate surfaces [132].

Protein C is a potential anti-coagulant. Activated protein C (APC), in conjunction with its cofactor protein S, functions to suppress coagulation by enzymatically degrading FVIIIa and FVa – activators of factor X and prothrombin, respectively [157]. Fibronectin, based on the presence or absence of fibrin, switches its function in platelet aggregation and thus provides a self-limiting mechanism that prevents excessive platelet accumulation and vessel occlusion [158]. Zero responses were exhibited by Protein C, Protein S, and fibronectin, indicating no effect of the presence or absence of UTXs and PEO chain densities on anticoagulant activity by these proteins for all surfaces. Protein C has not been detected in PEO-grafted polyurethane surfaces [132].

3.3.4.2 Immunological proteins

Complement C3 is crucial to the classical pathway, mannose-binding lectin pathway, and, notably, the alternative pathway, which is crucial in biomaterial-induced complement activation [30, 159-161]. C3 is identified in four separate bands: intact C3 (187 kDa), α chain (115 kDa), β chain (70 kDa), and an activation fragment (42 kDa). Intact C3 (187 kDa) and the α chain were not detected on almost all studied surfaces, with only a very faint band of intact C3 observed for the control and PEO 10 min in UTX-treated plasma. A very faint α chain band was also observed for PEO 10 min in UTX-treated plasma. Low to moderate amounts of β chains and activation fragments (except for control) were detected on all surfaces. UTX addition increased C3-mediated activation by all surfaces, most significantly for activation fragments on high-chain density surfaces. From Table 3.4 and Table 3.5, it is evident that more of this fragment was observed on all surfaces after UTX addition. Previous studies using normal plasma have shown low to relatively high adsorption levels of the C3 β chain (70 kDa) on Au surfaces coated with PEO of varying lengths and chain densities [36]. Studies conducted on segmented polyether urethanes modified with polyethylene oxide-polyurethane-polyethylene oxide block copolymers have shown that increasing the chain density of these copolymers on the surface decreased C3 adsorption [162].

IgG plays a critical role in humoral adaptive immunity, and its inclusion in the protein corona could greatly affect the activation of immune cells and the overall immune response [160]. IgG light (27 kDa) and heavy (55 kDa) chains were evaluated, and previous studies have indicated that the IgG light chain (27 kDa) was not detected on either Au control or PEO-modified surfaces. In contrast, the IgG heavy chain (55 kDa) has been observed to adsorb onto both Au control and PEO-modified surfaces [36]. The current study depicts low responses for both heavy and light

chains, with notable increase for the light chain on PEO 30 min sample upon UTX addition. This suggests that the IgG adsorption was somewhat independent of mPEO chain density and UTXs.

Transferrin (77 kDa) is associated with innate immunity and has been found to activate macrophages [161, 163, 164]. This protein has been found in protein corona eluted from PEO-grafted polyurethane surfaces [132]. There were low to no bands for transferrin across all surfaces, with no notable change upon adding UTXs.

Vitronectin helps facilitate cell adhesion to material surfaces [160, 165]. Despite similar plasma concentrations, investigations on different polystyrene-based surfaces have revealed that vitronectin exhibits a higher affinity for binding to surfaces compared to fibronectin [23, 166]. While vitronectin has been identified on PEO-grafted polyurethane surfaces, fibronectin has shown a slight decrease in adsorption to these surfaces compared to polyvinyl chloride and polymethyl methacrylate surfaces [132]. In this study, no visible band was identified for fibronectin or vitronectin in either normal or toxin-treated plasma except a faint band for mPEO 4 hr system incubated with normal plasma.

A weak band for α_1 antitrypsin, a potent inhibitor of coagulation, has previously been identified in PEO-grafted polyurethane surfaces incubated with normal human plasma [132]. Except for the PEO 10 min system, α_1 antitrypsin was not detected on any surfaces incubated with normal plasma. Faint bands were observed for the control and PEO 10 and 30 min systems when toxins were added to the plasma. α_2 macroglobulin is a serine protease inhibitor that can effectively inhibit a broad spectrum of proteases across various catalytic classes [161]. No detectable band was obtained for α_2 macroglobulin.

Table 3.6. Percent (%) change in protein band intensities of proteins attached to mPEO surfaces after UTX addition.

Plasma Proteins			Fragment size (kDa)	Au control	PEO 10 min	PEO 30 min	PEO 4 hr
	Albumin		66	50	37.5	50	-20
Immune response-related	C3:	Whole C3	187	appeared	appeared	absent	absent
		Chain α	115	absent	appeared	absent	absent
		Chain β	70	100	28.57	75	50
		Activation fragment	42	absent	16.66	66.66	300
	IgG:	Heavy chain	55	appeared	100	100	0
		Light chain	27	100	150	200	33.33
	Transferrin		77	appeared	-50	appeared	appeared
	Vitronectin		54	absent	absent	absent	-100
	α_1 antitrypsin		54	appeared	0	appeared	absent
Coagulation related	Fibrinogen:	α chain	68	400	200	100	-66.66
		β chain	56	400	-50	-60	-50
		γ chain	48	200	0	-50	0
	Prothrombin		72	absent	-100	appeared	appeared
	Factor XI		70	0	-50	0	-55.55
	Plasminogen		91	appeared	absent	absent	absent

Color scale: % increase | % decrease | appeared

Table 3.6 represents the % change in protein band intensities after UTX addition. The dark green and red colors illustrate the percent increase and decrease in band intensities respectively, upon UTX addition. The light green color represents the absent proteins that appeared after UTX introduction. '0' indicates that protein intensities did not change. It is clear from the above table that UTXs either increased the adsorption to mPEO surfaces or made the absent proteins appear, more than the decline they caused in band intensities.

3.4 Conclusion

We evaluated the effect of end-tethered mPEO chain density and UTXs on plasma protein adsorption using immunoblots. Albumin and activation fragment of complement C3 exhibited maximum intensity change upon UTX addition for PEO 30 min surfaces. Apart from this, almost all proteins increased in adsorbed amounts upon introducing UTXs. Metabolites have been shown to affect protein conformation and enzymatic function. However, it is unknown whether the increased protein presence at the blood-biomaterial interface directly affects biological function or is only a result of protein denaturation. Thus, the effect of toxins on blood proteins and their interactions with engineered surfaces should not be overlooked when considering the design of blood-contacting materials for ESKD patients. On the other hand, the effect of different chain densities was subtle. For UTX plasma, fibrinogen and factor XI show a notable decrease in band intensities for PEO 10 min, PEO 30 min, and PEO 4 hr samples, with respect to UTX-Au control, proving a sustained ability for PEO to reduce some protein adsorption even with UTX presence. However, not all proteins show reduced adsorption with increased PEO chain density, making the adsorption behaviors less obvious and enhancing the need to understand PEO-mediated protein resistance in depth. Although the chain densities did not differ statistically for 10 min and 30 min chemisorption times, the protein adsorption data did, indicating a sharp transition in protein resistance with varying PEO chain density. It is evident from the above findings that the presence of UTXs impacts non-specific plasma protein adsorption to mPEO-modified surfaces and should not be overlooked when considering the design of blood-contacting biomaterials for this patient group.

Chapter 4. Effect of hydroxy-PEO chain density and uremic toxins on plasma protein adsorption[2]

4.1 Introduction

Protein adsorption at biomedical device surfaces is the impetus for deleterious host responses to blood-contacting biomaterials [3, 4]. Films of end-tethered polyethylene oxide (PEO) are the gold standard for inhibiting nonspecific protein adsorption at the blood-biomaterial interface [4]. The low-fouling attributes of these PEO films are associated with several properties, including hydrogen bonding, hydrophilicity, electrical neutrality, hydrogen bond acceptance, chain conformation, and chain density [36, 40, 41, 48, 136]. PEO interactions with water and surface hydrophilicity affect protein adsorption [[45], [46, 47, 167-169]]. Previous work has shown that hydroxy-terminated PEO-modified surfaces begin to level off the lysozyme adsorption at the chain density of ~0.5 chains/nm^2 [48]. Similarly, methoxy-terminated PEO-modified surfaces showed optimum reduction in fibrinogen adsorption at the same chain density [37, 48]. Despite extensive research on protein adsorption to PEO-modified surfaces, the vast majority use only blood from healthy donors, neglecting the changes in the blood that occur in unhealthy patients [139-141]. Metabolomics research has illuminated how dynamic the composition of blood is, and how it is significantly influenced by the type of disease and its underlying pathogenesis [70, 79].

Kidney failure is associated with a reduced glomerular filtration rate (< 60 mL/min/1.73 m^2) and leads to the retention of uremic toxins (UTX) in blood [68, 69]. Some UTXs, especially the protein-bound uremic toxins (PBUTs), are extremely difficult to remove through membrane

[2] This chapter has been submitted as Aishwarya S Pawar[1], Ayda Ghahremanzadeh[2], Mehdi Ghaffari Sharaf[2], Larry D Unsworth[*], Effect of hydroxy-PEO chain density and uremic toxins on plasma protein adsorption, for publication in the Colloids and Surfaces A: Physicochemical and Engineering aspects.

hemodialysis, and their blood concentrations are quickly re-established due to their release from blood proteins [77]. Many of the UTXs, including uridine, hippuric acid, putrescine, and indole acetic acid, have been recognized for their toxicity, and their concentrations under normal and pathological conditions have been quantified [79, 80]. UTX-protein interactions have been found to modify protein adsorption patterns to surfaces through interacting with surfaces and blood proteins [1, 69, 77, 81]. However, limited work in this field exists, and mechanisms behind the alteration in protein-surface interactions remain ill-defined. Indoxyl sulfate and p-cresol sulfate have been reported to form electrostatic and hydrophobic interactions with human serum albumin and alter its secondary and tertiary structures [77]. UTXs have been reported to cause protein-folding events [82]. PBUTs like indoxyl sulfate, p-cresol sulfate, urea, and creatinine have also been studied for their direct adsorption to various surfaces, including polydopamine and amine-functionalized mesoporous silica [89, 90]. It was found that the pyrene-modified MOF exhibited the highest adsorption of p-cresol sulfate, indoxyl sulfate, and hippuric acid from a group of zirconium-based metal-organic frameworks (MOFs) [170]. The modification of activated carbon with sulfuric acid increased the toxins' adsorption, especially urea and creatinine, by 30 to 40 % [95]. Synthetic polymers, including polyvinylpyrrolidones, polysulfones, and polyamides, have also been widely used to adsorb uremic toxins [171, 172]. Adsorption of uremic toxins to 2-(methacryloyloxy)ethylphosphorylcholine-co-β-cyclodextrin (p(MPC-co-PMβCD)) films from a complex UTX solution, as published recently by our group, was the first attempt to elaborate β-CD's affinity for binding uremic toxins combined with their interaction with the well-known low-protein fouling MPC film [69]. The biocompatibility and protein adsorption experiments on p(PMβCD-co-MPC) modified magnetic nanoparticles as an innovative material for removing toxins from blood were performed [23], where UTXs slowed down the blood coagulation.

Nonetheless, the main objective of all these studies was to develop more effective adsorbents for toxin removal, whereas the present study focuses on how uremic toxins influence plasma protein adsorption to PEO-modified surfaces.

Uremic toxins can bind to even low-fouling polymer films [69], suggesting that not only do UTXs affect protein structures but also the surface properties responsible for inhibiting protein adsorption. Herein, we form thin chemisorbed films of hydroxy-terminated PEO (PEO-OH, 800 MW) with a range of polymer chain densities. Films were characterized for hydrophilicity and elemental composition as a function of polymer chain density. Normal platelet-poor plasma was altered by adding 25 uremic toxins in concentrations equivalent to those found in end-stage kidney disease patients (Table 4.1). Adsorbed proteins were eluted and characterized using immunoblotting techniques. It is thought that the next stage in the development of personalized medicine approaches for designing blood-contacting biomaterials must incorporate an understanding of how the changes in blood composition affect the blood-biomaterial interface.

Table 4.1. Composition of uremic toxins in HD patients. Values are concentration ± SD.

Uremic toxins	Experimental concentration (mg/L)	Patient concentration (mg/L)	Ref
4-Ethylphenyl sulfate	0.25	0.242 ± 0.044	[143]
Indole acetic acid	2.03	2.03 ± 0.38	[79]
L-Tyrosine	54.35	54.35 ± 16.3	[144]
Asymmetric dimethylarginine	0.38	0.385 ± 0.2884	[79]
Hypoxanthine	2	2.0 ± 1.6	[80]
Spermidine	0.096	0.097 ± 0.045	[79]
Argininic acid	0.075	0.08 + 0.056	[80]
3-Deoxyglucosone	1.7	1.7 ± 1.0	[80]
Homocysteine	8.1	8.1 ± 1.6	[80]
L-Asparagine	7.16	7.13 ± 3.7	[145]
Pyruvic acid	11.7	5∼11.7 ± 8.6	[146]
Trimethylamine N-oxide	7.5	7.49 ± 2.39	[147]
Creatinine	136.4	136.0 ± 46.0	[80]
Hippuric acid	237	247.0 ± 112	[80]
Uric acid	83	83 ± 13	[148]
Xanthosine	96.6	96.6 ± 62.9	[149]
Putrescine	0.001	0.00942 ± 0.00759	[79]
Uridine	9.8	9.8 ± 11.4	[80]
Dimethyl glycine	0.59	0.5768	[80]
Guanidinopropionic acid	0.288	0.288 ± 0.0183	[80]
p-Hydroxyhippuric acid	4.25	4.43 ± 2.79	[150]
Phenylalanine	9.25	8.92 ± 1.81	[151]
Indoxyl glucuronide	2.5	2.5 ± 0.3	[79]
Indoxyl sulfate	53	53.0 ± 91.5	[80]
Spermine	0.002	0.018 ± 0.0162	[80]

4.2 Materials and methods

Chemicals used to prepare UTX solution: Sigma Aldrich provided a diverse array of chemicals, including Asymmetric dimethylarginine (≥98%), Putrescine (≥98%), Pyruvic acid (≥98%), L-Asparagine (≥98%), Dimethylglycine (≥99%), Hippuric acid (≥98%), Spermine (≥97%), L-Tyrosine (≥99%), Guanidinopropionic acid (≥97.5%), Spermidine (≥99%), Homocysteine (≥98%), Indoxyl sulfate, Indoxyl glucuronide (≥98%), Xanthosine, Creatinine (≥98%), Hypoxanthine (≥99%), Uridine (≥99%), 3-Deoxyglucosone (≥75%), Uric acid (≥99%), Trimethylamine N-oxide (≥95%), 3-Indoleacetic acid (≥98%), and Phenylalanine (≥98%). L-

Argininic acid was obtained from Toronto Research Chemicals (Ontario, Canada). 4-Ethylphenyl sulfate (98%) was procured from Apex Bio (Houston, USA), while 4-Hydroxyhippuric acid (≥98%) was sourced from Cayman Chemical.

Chemicals used in experiments: Platelet-poor human plasma was obtained through the Blood4Research initiative facilitated by Canadian Blood Services. Polyvinylidene fluoride (PVDF) membrane and sodium dodecyl sulfate (SDS) were acquired from Bio-Rad (Hercules, CA, USA). PEO-OH (800 MW) was sourced from Biopharma PEG Scientific Inc. (Watertown, MA, USA). Tween 20, TEMED, β-mercaptoethanol, and glycine were sourced through Sigma Aldrich, nonfat dry milk (carnation dry milk), and colloidal gold solution and ladder solution were obtained from Bio-Rad labs, USA. HPLC-grade water, PBS tablets (pH 7.4), tris base, and 40% acrylamide were obtained from Fisher Scientific. The TMB-stabilized substrate was procured from Promega (Madison, WI, USA). All chemicals were utilized as received without additional purification. For the complete list of antibodies, please refer to Table B1 in Appendix B.

4.2.1. PEO chemisorption to surfaces

The variable PEO chain densities on gold surfaces were obtained by varying chemisorption time and altering chemisorption solution conditions. Using previously established protocol [37, 49, 152], a hydroxy-terminated, chain end thiolated, 5 mM PEO solution (800 g/mol) was prepared in 0.1 M PBS buffer (pH 7.4, ionic strength 4.4 M) under the low solubility conditions (usually θ conditions) near the cloud point. The silicon wafers (Thin Film Technology, Buellton, CA), coated with 500 Å chromium and 2000 Å gold, were diced into 0.5 x 0.5 cm chips and piranha washed as mentioned before [36] to remove any carbon-containing contaminants. The cleaned gold surfaces were immersed in HPLC-graded Milli-Q water and equilibrated at 25 °C for 30 min alongside a chemisorption solution in a non-adherent 96-well plate. The individual surfaces were subsequently

placed into chemisorption solutions of consistent volumes and incubated for varying durations (10 min, 30 min, and 4 hrs) at the same temperature to attain diverse PEO chain densities. The surfaces were rinsed with adequate HPLC-graded Milli-Q water post-chemisorption to remove loosely bound polymer, dried using inert N_2 gas, and used for further experiments.

4.2.2. PEO film characterizations

4.2.2.1 Measurement of dynamic contact angle

The Attension Theta Lite Optical Tensiometer (Nanoscience Instruments, USA) was used to characterize the dynamic contact angles of PEO-OH films. Advancing and receding water contact angles were measured by forming water drops on the surfaces, where the drops were permitted to advance and then recede on the chips for 40 seconds, during which the corresponding values were recorded. The instrumental parameters were set ensuring a drop-out volume not exceeding 2 μL and a controlled advancing/receding rate of 0.2 μL/s. Statistical significance between the obtained values was assessed using an unpaired Student's t-test.

4.2.2.2 Evaluation of PEO chain densities

After chemisorption onto surfaces, the thicknesses of the dried PEO-OH films were determined using a variable-angle M-2000V spectroscopic ellipsometer (J.A. Woollam, USA; 370–1000 nm). Provided software (CompleteEASE, J.A. Woollam, USA) was used to determine the extinction coefficient (k) and refractive index (n) by applying the B-spline model with a node spacing of 0.1 eV and using Au metal as a base. Following this, a Cauchy model was implemented to ascertain the thickness of the PEO layer using the optical constants of Au as substrates for the polymer films. Given the transparent nature of PEO, the Cauchy parameters were set to their lowest values (A = 1.45 and B = 0.01). Finally, the chain densities were determined based on the dry film properties using the provided equation:

$$L = \left(\frac{M}{\rho_{dry} d N_A}\right)^{1/2} \quad \text{Eq. 4.1}$$

In this equation, L represents the mean distance between polymer attachment points on the surface, M is the molecular weight of PEO, ρ_{dry} is the assumed dry PEO layer density (1.0 g/cm³), d is the mean layer-thickness obtained from ellipsometry, and N_A is Avogadro's number. The final polymer chain density is evaluated as L^{-2}. An unpaired Student's t-test was performed to analyze statistical differences between obtained grafting densities.

4.2.2.3 Elemental composition of polymer films

X-ray photoelectron spectroscopy (XPS) measurements at room temperature were conducted using the Kratos Axis (Ultra) spectrometer (Kratos Analytical Ltd, UK), equipped with monochromatized Al Kα X-rays (hυ = 1486.71 eV). The spectrometer was calibrated using the binding energy of Au 4f7/2 (84.0 eV) with reference to the Fermi energy level. Atomic compositions (%) were determined from a low-resolution survey spectrum spanning 0 to 1100 eV, collected at the analyzer with a pass energy of 160 eV. Spectral fitting employed CasaXPS software (Casa Software Ltd., Japan) for the quantification of elements in percentage.

4.2.3. Adsorption of plasma proteins

Human plasma experiments were conducted in accordance with the guidelines established by the research ethics board approvals: Canadian Blood Services 2022-21 and University of Alberta Pro00002363 and Pro00116764. The platelet-poor human plasma (collected from multiple donors) was used as received from Canadian Blood Services, aliquoted, and stored at -80 ºC. Protein adsorption from plasma was facilitated by following the previously developed protocol [36]. The PEO-modified surfaces were incubated in undiluted plasma for 3 hrs under static conditions at room temperature and washed three times (10 min each) with copious amounts of PBS buffer to remove

any loosely bound plasma proteins. Plasma incubation and serial washing of surfaces were carried out in individual wells of non-adherent 96-well plates to avoid an overlap of surfaces.

The protein adsorption protocol was the same for UTX plasma, except the plasma was encompassed with 25 different uremic toxins (Table 4.1) to achieve the blood composition of HD patients. A highly concentrated stock solution of 25 different uremic toxins (with concentrations equivalent to those in HD patients) was prepared, aliquoted, and stored at -80 ºC. Immediately prior to use, 1 mL plasma was added to each UTX vial, mixed with a pipette, and kept undisturbed for 30 min at room temperature to completely dissolve the UTXs.

4.2.4. Immunoblot technique

In this study, proteins eluted from surfaces after plasma incubations were analyzed using the standard sodium dodecyl sulfate-polyacrylamide gel electrophoresis (SDS-PAGE) and immunoblotting techniques. Surface adsorbed proteins were eluted by incubating surfaces in 2% SDS overnight at room temperature. Samples were sonicated for 2 min at room temperature each time before and after the elution. Prior to SDS-PAGE, eluted samples were denatured using a buffer composed of 0.5 M β-mercaptoethanol and SDS at 95 ºC for 5 min. Equal volumes (100 µL) of eluted samples were loaded onto each polyacrylamide gel (12 % separating, 4 % stacking). After electrophoresis, proteins were electrophoretically transferred to immobilon polyvinylidene fluoride (PVDF) membranes (Millipore, Bedford, MA) of pore size 0.2 µm. The consistent surface area of surfaces, elution buffer volume, and sample loading volume were maintained across all experiments to allow comparison between the blots. Following electro-transfer, the membrane was segmented into 22 strips, with 2 allocated for colloidal gold staining and the remaining 20 for immunoblotting to detect 20 individual proteins (Table B1, Appendix B). The strips were then probed with primary (1:1000 dilution) and alkaline phosphatase-conjugated affinity-purified secondary antibodies

(1:1000 dilution). The bands were visualized using a 3,3',5,5'-tetramethylbenzidine (TMB)-stabilized chromogen substrate (Promega), maintaining the constant color development time throughout all immunoblots. The strips were immediately dried, reassembled along with gold-stained strips, and converted to digital format. Band intensities were analyzed using ImageJ 1.53e, USA, and quantified using a 12-step grayscale system where '0' and '12' represented 'no band' and 'maximum intensities,' respectively.

4.3 Results and discussion

4.3.1. Hydrophilic properties of PEO films

Advancing and receding contact angle measurements for bare and PEO-OH-modified surfaces were conducted (Table 4.2). Statistical differences were calculated using the unpaired student's t-test. Contact angles decreased significantly ($p_{adv} = 0.0001$, $p_{rec} = 0.0004$) from bare to all PEO-OH modified surfaces, confirming the polymer presence and indicating the increased hydrophilic properties of surfaces. Data for PEO 10 and 30 min modified surfaces were not statistically significant, but were from 30 min to 4 hr chemisorption times ($p_{adv} = 0.0004$, $p_{rec} = 0.0007$).

Table 4.2. The advancing and receding contact angle values (°) of PEO-OH modified gold surfaces. Data are mean ± SD ($n \geq 3$).

Surface	Advancing (°)	Receding (°)
Unmodified Au	81.6 ± 1.2	74.3 ± 2.4
10 min PEO-OH modified	55.3 ± 1.2	49.3 ± 3.0
30 min PEO-OH modified	55.7 ± 1.2	44.1 ± 1.9
4 hr PEO-OH modified	38.2 ± 2.5	30.5 ± 1.7

4.3.2. PEO chain density

The PEO chain densities were assessed to examine polymer conformation (mushroom or brush) and to investigate the impact of varying grafting densities on protein adsorption. PEO-OH grafting densities of 0.56 ± 0.10, 0.57 ± 0.10, and 0.82 ± 0.13 chains/nm² were obtained after 10 min, 30 min, and 4 hr of formation time, respectively. It has been reported that for unperturbed random coils of polymer (mushroom conformation), the distance between polymer attachment points (S) is greater than twice the Flory radius (R_F) at θ condition [49]. The '$2R_F$' for PEO-OH was calculated to be 23.7 Å. The respective values of 'S' for 10 min, 30 min, and 4 hr PEO films were 13.3 Å, 13.2 Å, and 11 Å. It is clear from the values that for all time points, $S < 2R_F$, indicating the PEO layers were in the brush regime. In addition, the grafting density values obtained remained below the reported upper limit of 5.8 chains/nm² for fully extended polymer chains [49, 153], further confirming that PEO chains were in brush conformation. Chain densities under given chemisorption conditions remarkably increased with chemisorption time from 10 min (0.56 ± 0.10 chains/nm²) to 4 hr (0.82 ± 0.13 chains/nm²) and were statistically different ($p = 0.016$). However, similar to the results previously obtained for methoxy-PEO systems (in review), here the chain densities for PEO 10 min (0.56 ± 0.10 chains/nm²) and 30 min (0.57 ± 0.10 chains/nm²) were not significant ($p = 0.83$).

4.3.3. Elemental composition of PEO films

The atomic compositions obtained from low-resolution XPS data (Table 4.3) show that for unmodified gold, the carbon and oxygen content were found to be 27.5 and 10.3%, respectively, and represent atmospheric carbonaceous contamination [154]. The drastic reduction in gold content, coupled with the increase in carbon and oxygen levels from unmodified to modified samples [41], confirms the successful deposition of PEO on the surfaces. On modified surfaces

with increasing chain density, the decrease in gold content and increase in carbon and sulfur [49] levels further indicate a greater deposition of PEO as chain density increases. Sulfur serves as a distinct indicator of adsorbed thiolated PEO. The oxygen contents on all PEO samples were statistically similar. The C:O ratio increased with chain density for PEO-OH films, approaching the theoretical value of 1.9 for PEO-OH.

Table 4.3. Percent atomic compositions of PEO-OH films obtained from low-resolution XPS scan. Values are mean ±SD, n = 3.

Surface	Element composition (%)				
	Au 4f (83 eV)	O 1s (532 eV)	C1 s (285 eV)	S 2p (165 eV)	C:O
Unmodified gold	62.3 ± 4.5	10.3 ± 0.9	27.5 ± 4.2	0	2.7 ± 0.4
10 min PEO-OH modified	47.0 ± 1.5	22.0 ± 0.7	29.5 ± 1.6	1.6 ± 0.4	1.3 ± 0.1
30 min PEO-OH modified	43.1 ± 0.6	22.0 ± 1.3	33.1 ± 1.3	1.8 ± 0.2	1.5 ± 0.1
4 hr PEO-OH modified	41.0 ± 0.7	22.2 ± 0.9	34.4 ± 1.4	2.5 ± 0.1	1.6 ± 0.1

4.3.4. Adsorbed protein analysis

Eluted proteins from all surfaces were characterized using immunoblot techniques and band intensities summarized in Table 4.4 and Table 4.5. Complement C3, albumin, and factor XI were detected on all immunoblots with amounts (i.e., intensities) that were affected by the presence of UTXs and variable chain densities. Unlike methoxy-terminated PEO surfaces of similar chain densities (in review), no proteins reached the maximum band intensity value (12). This is likely due to the increased propensity for hydrophilic -OH groups to present at the PEO-plasma interface as chain density increases [48]. As the "-OH" group is more hydrophilic than the corresponding methoxy group, protein adsorption is not as high.

Albumin (66.5 kDa) is a high concentration plasma protein (35-50 g/L) that binds diverse lipids, metabolic compounds, and drugs [23, 70, 173]. In the present work, it appeared in intermediate to high intensities, similar to the previous work on PEO-OH-modified gold surfaces [36]. For normal plasma, the PEO-modified surfaces displayed similar or higher [36] band intensities than the control. Upon UTX addition, albumin intensities for PEO-modified surfaces declined significantly from that of UTX-Au control. It is known that 90% of indoxyl sulfate (IS) in the bloodstream can reversibly bind to albumin with a dissociation constant of 13.2 μM [70, 174-176]. The highest band intensity throughout the immunoblots was observed on UTX-Au control samples. While UTXs increased albumin adsorption to Au control, they significantly decreased the adsorption to PEO 10 min surfaces. The intensities for PEO 30 min and 4 hr surfaces for both normal and UTX plasma were identical, indicating the adsorption on these surfaces was independent of UTX effects and chain density variations. However, for PEO 10 and 30 min surfaces, although the chain densities were not statistically significant ($p = 0.83$), the adsorption data varied for both normal and UTX plasma. PEO 4 hr samples from normal plasma and PEO 10 and 30 min samples from UTX plasma exhibited significantly lower albumin intensities compared to our previous study on methoxy-PEO-modified surfaces (in review). This suggests that surface modification with PEO-OH more effectively resists albumin adsorption compared to methoxy-PEO.

4.3.4.1 Immune response-related proteins

IgG is the most prevalent circulating antibody isotype (10 to 20% of proteins in plasma) within the immunoglobulin superfamily and is the key element of humoral adaptive immunity [160]. Two separate bands, light (27 kDa) and heavy chain (55 kDa) characterize the presence of IgG. It has been detected previously on PEO-modified polyurethane surfaces [132]. Despite being

the most abundant protein, IgG was minimally detected on all surfaces. This was consistent with previous work on PEO-OH chemisorbed gold surfaces [36]. The intensity values for both normal and UTX plasma were consistently low, indicating that neither variable chain densities nor the UTXs influenced the adsorption of this protein. For UTX plasma, the IgG light chain intensity for PEO 10 min surfaces was considerably lower than that obtained for methoxy-PEO surfaces (in review), confirming that the end-group at these conditions does affect protein adsorption.

Table 4.4. Relative immunoblot intensities of plasma proteins adsorbed to surfaces of varying PEO chain densities. The values range from 0, indicating no visible band, to 12, indicating a band with maximum intensity.

	Plasma Proteins		Fragment size (kDa)	Au control	PEO 10 min	PEO 30 min	PEO 4 hr	
	Albumin		66	6	8	6	6	0
								1 to 3
Immune response-related	C3:	Intact C3	187	0	1	1	1	4 to 5
		α chain	115	0	1	1	1	6 to 7
		β chain	70	1	9	9	6	8 to 9
		Activation fragment	42	0	5	5	3	10 to 11
	IgG:	Heavy chain	55	0	1	2	1	12
		Light chain	27	1	3	3	3	
	Transferrin		77	0	0	0	1	
	Vitronectin		54	0	0	0	0	
	α_1 antitrypsin		54	0	0	0	0	
	α_2 macroglobulin		163	0	0	0	0	
Coagulation related	Fibrinogen:	α chain	68	1	2	0	1	
		β chain	56	1	1	0	1	
		γ chain	48	1	1	0	0	
		Cleavage fragments	<48	0	0	0	0	
	Fibronectin		259	0	0	0	0	
	Prothrombin		72	0	0	0	0	
	Antithrombin		53	0	0	0	0	
	Factor XII		80	0	0	0	0	
	Factor XI		70	7	6	6	6	
	Kininogen (heavy)		120	0	0	0	0	
	Protein C		62	0	0	0	0	
	Protein S		75	0	0	0	0	
	Prekallikrein		85	0	0	0	0	
	Plasminogen		91	0	0	0	0	

Table 4.5. Relative immunoblot intensities of plasma proteins adsorbed to surfaces of varying PEO chain densities in the presence of uremic toxins. The values range from 0, indicating no visible band, to 12, indicating a band with maximum intensity.

	Plasma Proteins		Fragment size (kDa)	UTX-Au control	UTX-PEO 10 min	UTX-PEO 30 min	UTX-PEO 4 hr
	Albumin		66	9	4	6	6
Immune response-related	C3:	Intact C3	187	1	1	2	1
		α chain	115	0	1	0	0
		β chain	70	2	6	2	4
		Activation fragment	42	0	6	2	4
	IgG:	Heavy chain	55	1	2	1	1
		Light chain	27	2	2	2	3
	Transferrin		77	1	0	0	0
	Vitronectin		54	0	0	0	0
	α_1 antitrypsin		54	1	0	0	0
	α_2 macroglobulin		163	0	0	0	0
Coagulation related	Fibrinogen:	α chain	68	5	1	1	1
		β chain	56	5	1	1	1
		γ chain	48	3	1	1	1
		Cleavage fragments	<48	0	0	0	0
	Fibronectin		259	0	0	0	0
	Prothrombin		72	0	0	0	0
	Antithrombin		53	0	0	0	0
	Factor XII		80	0	0	0	0
	Factor XI		70	7	2	2	2
	Kininogen (heavy)		120	0	0	0	0
	Protein C		62	0	0	0	0
	Protein S		75	0	0	0	0
	Prekallikrein		85	0	0	0	0
	Plasminogen		91	1	0	0	0

Complement C3 plays a crucial role in all three activation pathways—classical, alternative, and mannose-binding lectin pathway. It particularly functions in the alternative pathway, where it contributes to complement activation induced by biomaterials [30, 161]. C3 is recognized as three distinct bands - intact C3 (187 kDa), α chain (115 kDa), β chain (70 kDa), and an activation fragment at 42 kDa. In the present work, the blot responses for intact C3 and α chain were negligible for normal plasma. Studies on PEO-OH-modified surfaces detected moderate and high amounts of β chain and an activation fragment, respectively [36]. Here, the β chain obtained the highest intensities on low chain density surfaces (PEO 10 min and PEO 30 min) but adsorbed weakly to the high chain density surface (PEO 4 hr) in normal plasma, indicating reduced adsorption with increasing chain density. The moderately present activation fragment for both normal and UTX plasma suggests C3 degradation. The introduction of UTXs significantly declined β chain adsorption to PEO 10 and 30 min surfaces. For UTX plasma, the adsorption of β chain and activation factor increased with increasing chain density from PEO 30 min to PEO 4 hr surfaces. For UTX plasma, the adsorption of β chain and activation factor dropped significantly from PEO 10 min to PEO 30 min surfaces, although the chain densities were statistically similar ($p = 0.83$). This indicated that the adsorption was highly sensitive to chain density effects. Compared to previously obtained study on methoxy-PEO surfaces (in review), the β chain intensity for PEO 30 min samples obtained here for normal plasma was higher. However, for the UTX plasma, all PEO-modified surfaces exhibited lower adsorption of the β chain than their methoxy analogs. Similarly, C3 activation fragment adsorption to PEO 30 min and 4 hr surfaces was notably lower than their methoxy analogs, further confirming the better protein-resistant properties of the ‘hydroxy’ group.

Transferrin (single band - 77 kDa) plays a crucial role in innate immunity and can potentially activate macrophages [164]. It was scarcely present on all surfaces, aligning with the previous

research on transferrin as a coating on polystyrene nanoparticles, where it effectively reduced nonspecific protein adsorption from human plasma solutions [177]. Minimally detected transferrin, together with the low level of IgG, indicated low phagocytic activity on all surfaces. Transferrin adsorption wasn't influenced by either the inclusion of toxins or varied chain densities.

Vitronectin (54 kDa) is a multifunctional glycoprotein that greatly contributes to facilitating cell adhesion onto material surfaces along with fibrinogen and fibronectin [160, 165]. Although their plasma concentrations are similar, studies on various polystyrene-based surfaces have shown that vitronectin displays a greater affinity for surface binding compared to fibronectin [23, 166]. Zero responses were obtained for vitronectin and fibronectin, which implies that these proteins did not provide a propensity for cells to bind to any of the surfaces.

α_1 antitrypsin is a serine protease inhibitor that acts by regulating enzymes linked to inflammation, specifically neutrophil elastase [178]. It was found to be adsorbed weakly on the PEO-grafted polyurethane surface before [132]. No visible responses for this protein were obtained. Identical blot responses were observed for α_2 macroglobulin, another element of the innate immune system that regulates proteases by removing them from the bloodstream [23, 179, 180]. The absence of α_2 macroglobulin implies that PEO-OH-modified surfaces, even when exposed to UTXs, are not actively promoting clotting or fibrinolysis, given its role as an inhibitor for both processes [23, 181].

4.3.4.2 Coagulation-related proteins

Fibrinogen is an essential protein in blood clotting and is a site for three coagulation-related enzymes - plasmin, thrombin, and factor XIIIa. Fibrinogen presents as three bands: α (68 kDa), β (56 kDa), and γ (48 kDa), and a cleavage fragment at <48 kDa. It has been detected in a range of intensities in previous research on PEO-OH grafted gold surfaces [36]. Fibrinogen was found to be strongly attached to PEO-grafted polyurethane surfaces [132]. However, in the present study, it was

found in minimal quantities with no visible band on PEO 30 min samples. UTX presence led to increased intensities for the Au controls relative to normal plasma. However, UTXs did not alter the adsorption of PEO-modified surfaces. For UTX plasma, a notable decline in band intensities was observed from UTX-Au control to all PEO-modified surfaces. The low and consistent fibrinogen intensities on PEO-modified samples for UTX plasma indicated that protein resistance was independent of varying chain densities. No activation fragments were detected for normal or UTX plasma. For normal plasma, while α and β chains for PEO 30 min surfaces previously showed moderate intensities on methoxy-PEO modified surfaces (in review), they were absent in the present work. Similarly, for UTX-plasma, the α chain for PEO 10 and 30 min surfaces exhibited markedly lower adsorption than their methoxy analogs.

The contact coagulation pathway integrates the non-enzymatic cofactor high-molecular-weight kininogen and three serine proteinases: Factors XII and XI and prekallikrein [23, 156]. Low and negligible amounts of these proteins were detected previously on PEO-OH-modified gold surfaces [36] and PEO-grafted polyurethane-based adsorption systems [132]. High-molecular-weight kininogen adsorption was found to be reduced with PEO modification of surfaces [36]. For normal plasma, intermediate amounts of factor XI (70 kDa) were detected on all surfaces. For both normal and UTX plasma, consistent band intensities were obtained for all chain densities, indicating factor XI adsorption was unaffected by chain density effects. The consistency in responses can be correlated to the previous study on PEO-grafted surfaces, where the protein adsorption stabilized once the chain density reached 0.5 chain/nm^2 [48]. The chain densities obtained in the present work are greater than this threshold. Upon the introduction of toxins, the intensities of factor XI on PEO-modified surfaces reduced significantly yet consistently. While factor XI adsorption to PEO 30 min surface is more than that on methoxy-PEO modified samples studied earlier (in review), the

adsorption to PEO 4 hr surfaces here has reduced substantially. Other contact coagulation proteins - high MW kininogen (120 kDa), factor XII (80 kDa), and prekallikrein (85 kDa) were absent on all surfaces, indicating that the contact coagulation did not occur by these proteins.

While the presence of adsorbed proteins can offer insights into the host reactions to biomaterials, the absence of proteins also provides valuable information. The protein C (62 kDa) controls blood coagulation by regulating FVIIIa and FVa, key cofactors in factor X and prothrombin activation, respectively [157]. Similarly, protein S (75 kDa) acts as an anticoagulant by inhibiting procoagulants like FXa, FVa, and FIXa while supporting activated protein C and tissue factor pathway inhibitor [182]. Fibronectin (259 kDa) binds to fibrin through non-covalent and covalent interactions and regulates platelet function and hemostasis [23, 183]. Protein C, protein S, and fibronectin were absent throughout the immunoblots, indicating a limited fibrinolytic response and no anticoagulation activity by these proteins.

This trend continues for prothrombin (72 kDa) and antithrombin (53 kDa). Prothrombin exists as the inactive precursor to thrombin, a potent coagulation enzyme [161], whereas antithrombin is a potent serine protease inhibitor with the ability to deactivate thrombin and numerous enzymes within the coagulation cascade [184]. Low levels of prothrombin were observed previously on PEO-grafted polyurethane surfaces, whereas its adsorption to polyvinyl chloride and polymethyl methacrylate surfaces was comparatively higher [132]. While prothrombin facilitates thrombin-mediated coagulation, antithrombin prevents it. Zero responses were obtained for these proteins, eventually suggesting that the coagulation was neither promoted nor inhibited by any of the surfaces.

Plasminogen (91 kDa) undergoes a complex activation process to yield plasmin, a potent serine protease that enzymatically degrades fibrin clots [161]. Its appearance within the adsorbed proteome suggests the likelihood of fibrinolytic activity, a feature actively pursued in the advancement of other biomaterial surfaces [161, 185, 186]. In a study, plasminogen exhibited weak responses for PEO-grafted polyurethane surfaces, whereas it adhered strongly to polymethyl methacrylate and polyvinyl chloride surfaces [132]. The lack of this protein in blots indicated that no fibrinolytic activity was induced *via* plasminogen on surfaces.

Table 4.6: % change in the band intensities of protein adsorbed to PEO-OH surfaces after UTX addition.

	Plasma Proteins		Fragment size (KD)	Au control	PEO 10 min	PEO 30 min	PEO 4 hr
	Albumin		66	50	-50	0	0
Immune response-related	C3:	Whole C3	187	appeared	0	100	0
		Chain α	115	absent	0	-100	-100
		Chain β	70	100	-33.33	-77.78	-33.33
		Activation fragment	42	absent	20	-60	33.33
	IgG:	Heavy chain	55	appeared	100	-50	0
		Light chain	27	100	-33.33	-33.33	0
	Transferrin		77	appeared	absent	absent	-100
	α_1 antitrypsin		54	appeared	absent	absent	absent
Coagulation related	Fibrinogen:	α chain	68	400	-50	appeared	0
		β chain	56	400	0	appeared	0
		γ chain	48	200	0	appeared	appeared
	Factor XI		70	0	-66.66	-66.67	-66.66
	Plasminogen		91	appeared	absent	absent	absent

Color scale: % increase | % decrease | appeared

Table 4.6 represents the % change in protein band intensities after the introduction of UTX. The dark green and red areas indicate the percentage increase and decrease in band intensities, respectively, following the addition of UTX. The light green color represents proteins that were initially absent but became detectable after UTX was introduced. A '0' signifies no change in protein intensity. From the table, it is evident that UTX readily influenced the adsorption to PEO-OH surfaces.

4.4 Conclusion

We evaluated the effect of normal and UTX-laden plasma on the adsorption of proteins to PEO-OH-modified surfaces with different chain densities. The results revealed that albumin, complement C3, and factor XI were primarily detected on the blots, with minor traces of fibrinogen and IgG. It was observed that albumin and fibrinogen exhibited increased adsorption to the Au control upon UTX addition. While albumin adsorption increased from that of Au control to PEO 10 min samples, this trend was reversed in the presence of UTXs. UTXs markedly diminished the Factor XI appearance on all PEO-OH surfaces. The absence of high-molecular-weight kininogen, factor XII, and prekallikrein indicated surfaces generated no contact coagulation activity. The lack of prothrombin and antithrombin ultimately suggested that the PEO-modified surfaces neither facilitated nor inhibited clot formation. Many other coagulation-related proteins - protein C, protein S, and plasminogen exhibited zero responses on all surfaces. The prominent immune response-related protein, complement C3, showed an exclusive decline for the beta chain adsorption on PEO 30 min samples upon UTX addition. The negligible adsorption of transferrin and α_1 antitrypsin combined with the lack of vitronectin and α_2 macroglobulin indicated trivial immune responses generated by surfaces, which were independent of chain density and uremic toxins. Overall, the effect of UTXs was recognizable in altering the adsorption of plasma proteins.

Although no overall trend was observed upon UTX addition, their influence on the ratio of individual adsorbed proteins was apparent. From UTX-PEO 10 min to UTX-PEO 30 min samples, the adsorption of complement C3 β chain and activation fragment notably declined, indicating adsorption was highly sensitive to even small changes in chain density. The adsorption of complement C3 β chain and activation fragment reduced with increasing chain densities from PEO 30 min to PEO 4 hr surfaces. However, this pattern was reversed when UTXs were added, making the high chain density surface adsorb more proteins. This suggests that an increase in polymer chain densities doesn't always lead to improved antifouling properties of the surface. Also, it remains unclear whether any increase in protein adsorption alters their biological functions. Thus, a more detailed and extensive understanding of how the UTX composition affects protein structure and function upon adsorption may be needed. Finally, this is the first step in understanding how UTXs affect protein adsorption at the blood-biomaterial interface forming a foundation for further studies in developing personalized approaches for dialysis.

Chapter 5. Conclusion and major contributions

The potential effect of uremic toxins (UTXs) and variable chain densities of end-tethered polyethylene oxide (PEO) on plasma protein adsorption was quantitatively evaluated in the present dissertation. Two distinct chain end-groups of PEO, methoxy ($-OCH_3$) and hydroxy (-OH) were used. The hydrophilicity, grafting densities, and atomic compositions of polymer films were assessed using dynamic contact angle, spectroscopic ellipsometry, and X-ray photoelectron spectroscopy, respectively. These characterizations confirmed that polymer hydrophilicity and chain densities increased with chemisorption time, all polymers were in brush conformations, and PEO deposition was successful. However, the dynamic contact angles and chain densities obtained for 10 and 30 min chemisorption times for both methoxy and hydroxy terminal groups attained were statistical similar. In immunoblotting experiments, major proteins identified on all surfaces included albumin, complement C3, IgG, fibrinogen, and factor XI. Trace amounts of α_1 antitrypsin, prothrombin, transferrin, and vitronectin were also detected in select samples. The complete absence of several thrombogenic and immunogenic proteins suggested the lack of host responses by adsorption of those proteins. For both methoxy and hydroxy-PEO-modified samples, the variations in chain densities and the presence of UTXs notably altered the adsorption of individual proteins. However, for hydroxy-PEO-modified surfaces, the overall band intensities were lower than their methoxy analogs, and none of the proteins attained the maximum band intensity value (12). This is likely attributable to the increased hydration associated with hydroxy groups compared to methoxy groups, leading to a consequent diminish in protein adsorption and better protein-resistant properties.

In the case of the methoxy-PEO-modified surfaces (chapter 3), nearly all proteins showed increased adsorption upon the introduction of uremic toxins (UTXs). Metabolites are known to

influence protein conformation and enzymatic function; however, it is unclear whether the increased protein at the blood-biomaterial interface directly impacts biological function or results from protein denaturation. Therefore, when designing blood-contacting materials for kidney disease patients, it is crucial to consider the impact of toxins on blood proteins and their interactions with engineered surfaces. On the other hand, although the effect of chain densities did not exhibit a trend, it was subtle. PEO with varying chain densities succeeded in resisting specific proteins even in the presence of UTXs. However, increased PEO chain density did not reduce the adsorption of all proteins. For several proteins, the negligible variations in chain densities resulted in a sharp transition in their adsorbed amounts, indicating protein adsorption was highly sensitive to chain density.

In the case of hydroxy-PEO-modified surfaces (chapter 4), while no consistent trend emerged with UTX addition, their impact on the relative ratios of individual adsorbed proteins was evident. Similar to methoxy-PEO, adsorption was sensitive to small changes in chain density. Conversely, for some proteins, the adsorption was independent of both UTX and chain density effects. For complement C3 β chain and activation fragment, UTXs made high chain density surfaces to adsorb more protein, indicating that higher polymer chain densities do not always enhance the antifouling properties of the surface.

Herein, we underscore the need for a deeper understanding of how PEO chain density mediates protein resistance. It also reveals the need for a deeper and more comprehensive understanding of how UTXs influence protein adsorption. The outcomes of this study are advantageous in developing a standard protein adsorption profile for the advancement of low-fouling surfaces for blood-contacting biomaterials. Moreover, they are valuable in the pursuit of personalized dialysis for people with kidney failure.

References

1. Chetwynd, A.J. and I. Lynch, The rise of the nanomaterial metabolite corona, and emergence of the complete corona. Environmental Science: Nano, 2020. **7**(4): p. 1041-1060.
2. Hu, W.-J., et al., Molecular basis of biomaterial-mediated foreign body reactions. Blood, The Journal of the American Society of Hematology, 2001. **98**(4): p. 1231-1238.
3. Yu, Q., et al., Anti-fouling bioactive surfaces. Acta biomaterialia, 2011. **7**(4): p. 1550-1557.
4. Zhang, H. and M. Chiao, Anti-fouling coatings of poly (dimethylsiloxane) devices for biological and biomedical applications. Journal of medical and biological engineering, 2015. **35**: p. 143-155.
5. Bahniuk, M.S., Human Plasma Adsorption to Biomaterials: Fundamental Level Chemical Modifications and Their Effects on Biocompatibility, in Department of Biomedical Engineering University of Alberta. 2017, University of Alberta.
6. Vroman, L., et al., Interaction of high molecular weight kininogen, factor XII, and fibrinogen in plasma at interfaces. 1980.
7. Unsworth, D.L.D., Protein Adsorption To Chemisorbed PEO Thin Films, in Chemical Engineering. 2005, McMaster University: Hamilton, Ontario.
8. Malmsten, M., Biopolymers at interfaces. 1st ed. 1998: CRC Press. 672.
9. Norde, W., Driving forces for protein adsorption at solid surfaces. Biopolymers at interfaces, 2003. **110**: p. 21-45.
10. Israelachvili, J.N., Intermolecular and surface forces. 2011: Academic press.

11. Schmidt, D.R., H. Waldeck, and W.J. Kao, Protein adsorption to biomaterials. Biological interactions on materials surfaces: Understanding and controlling protein, cell, and tissue responses, 2009: p. 1-18.

12. Grover, S.P. and N. Mackman, Intrinsic pathway of coagulation and thrombosis: Insights from animal models. Arteriosclerosis, thrombosis, and vascular biology, 2019. **39**(3): p. 331-338.

13. Furie, B. and B.C. Furie, The molecular basis of blood coagulation. Cell, 1988. **53**(4): p. 505-518.

14. Jaffer, I., et al., Medical device-induced thrombosis: what causes it and how can we prevent it? Journal of Thrombosis and Haemostasis, 2015. **13**: p. S72-S81.

15. Ziats, N., et al., Adsorption of Hageman factor (factor XII) and other human plasma proteins to biomedical polymers. The Journal of laboratory and clinical medicine, 1990. **116**(5): p. 687-696.

16. Mulzer, S. and J. Brash, Identification of plasma proteins adsorbed to hemodialyzers during clinical use. Journal of biomedical materials research, 1989. **23**(12): p. 1483-1504.

17. Yau, J.W., et al., Mechanism of catheter thrombosis: comparison of the antithrombotic activities of fondaparinux, enoxaparin, and heparin in vitro and in vivo. Blood, The Journal of the American Society of Hematology, 2011. **118**(25): p. 6667-6674.

18. Larsson, M., et al., A factor XIIa inhibitory antibody provides thromboprotection in extracorporeal circulation without increasing bleeding risk. Science translational medicine, 2014. **6**(222): p. 222ra17-222ra17.

19. Elam, J.-H. and H. Nygren, Adsorption of coagulation proteins from whole blood on to polymer materials: relation to platelet activation. Biomaterials, 1992. **13**(1): p. 3-8.

20. Van der Kamp, K. and W. Van Oeveren, Factor XII fragment and kallikrein generation in plasma during incubation with biomaterials. Journal of biomedical materials research, 1994. **28**(3): p. 349-352.

21. Mackman, N., R.E. Tilley, and N.S. Key, Role of the extrinsic pathway of blood coagulation in hemostasis and thrombosis. Arteriosclerosis, thrombosis, and vascular biology, 2007. **27**(8): p. 1687-1693.

22. Robertson, S. and M.R. Miller, Ambient air pollution and thrombosis. Particle and fibre toxicology, 2018. **15**: p. 1-16.

23. Li, S., et al., Hemocompatibility of β-Cyclodextrin-Modified (Methacryloyloxy) ethyl Phosphorylcholine Coated Magnetic Nanoparticles. Biomolecules, 2023. **13**(8): p. 1165.

24. Cesarman-Maus, G. and K.A. Hajjar, Molecular mechanisms of fibrinolysis. British journal of haematology, 2005. **129**(3): p. 307-321.

25. Risman, R.A., et al., Fibrinolysis: an illustrated review. Research and Practice in Thrombosis and Haemostasis, 2023. **7**(2): p. 100081.

26. Hoylaerts, M., et al., Kinetics of the activation of plasminogen by human tissue plasminogen activator. Role of fibrin. Journal of Biological Chemistry, 1982. **257**(6): p. 2912-2919.

27. De Simone, I., et al., A Novel Plasminogen Activator Anti-Fibrin-uPA Increases the Sensitivity of the Plasmin Generation Assay to Therapeutic Target PAI-1. Blood, 2023. **142**: p. 5464.

28. Chapin, J.C. and K.A. Hajjar, Fibrinolysis and the control of blood coagulation. Blood reviews, 2015. **29**(1): p. 17-24.

29. Dunkelberger, J.R. and W.-C. Song, Complement and its role in innate and adaptive immune responses. Cell research, 2010. **20**(1): p. 34-50.

30. Andersson, J., et al., Binding of C3 fragments on top of adsorbed plasma proteins during complement activation on a model biomaterial surface. Biomaterials, 2005. **26**(13): p. 1477-1485.

31. Janeway, C., et al., Immunobiology: the immune system in health and disease. Vol. 2. 2001: Garland Pub. New York.

32. Hourcade, D.E., Properdin and complement activation: a fresh perspective. Current drug targets, 2008. **9**(2): p. 158-164.

33. Craddock, P.R., et al., Complement and leukocyte-mediated pulmonary dysfunction in hemodialysis. New England Journal of Medicine, 1977. **296**(14): p. 769-774.

34. Noris, M. and G. Remuzzi. Overview of complement activation and regulation. in Seminars in nephrology. 2013. Elsevier.

35. Anderson, J.M., A. Rodriguez, and D.T. Chang. Foreign body reaction to biomaterials. in Seminars in immunology. 2008. Elsevier.

36. Unsworth, L.D., H. Sheardown, and J.L. Brash, Polyethylene oxide surfaces of variable chain density by chemisorption of PEO-thiol on gold: adsorption of proteins from plasma studied by radiolabelling and immunoblotting. Biomaterials, 2005. **26**(30): p. 5927-5933.

37. Unsworth, L.D., H. Sheardown, and J.L. Brash, Protein resistance of surfaces prepared by sorption of end-thiolated poly (ethylene glycol) to gold: effect of surface chain density. Langmuir, 2005. **21**(3): p. 1036-1041.

38. Browning, M., et al., Determination of the in vivo degradation mechanism of PEGDA hydrogels. Journal of Biomedical Materials Research Part A, 2014. **102**(12): p. 4244-4251.

39. Rufin, M.A., et al., Protein resistance efficacy of PEO-silane amphiphiles: Dependence on PEO-segment length and concentration. Acta biomaterialia, 2016. **41**: p. 247-252.

40. Ostuni, E., et al., Self-assembled monolayers that resist the adsorption of proteins and the adhesion of bacterial and mammalian cells. Langmuir, 2001. **17**(20): p. 6336-6343.

41. Wang, M., Effect of metabolites on protein adsorption to PEO films. 2021.

42. Ngo, B.K.D. and M.A. Grunlan, Protein resistant polymeric biomaterials. 2017, ACS Publications.

43. Napper, D.H., Polymeric stabilization of colloidal dispersions. (No Title), 1983.

44. McPherson, T.B., S.J. Lee, and K. Park, Analysis of the prevention of protein adsorption by steric repulsion theory. 1995, ACS Publications.

45. Vogler, E.A., Water and the acute biological response to surfaces. Journal of Biomaterials Science, Polymer Edition, 1999. **10**(10): p. 1015-1045.

46. Chen, S., et al., Strong resistance of phosphorylcholine self-assembled monolayers to protein adsorption: insights into nonfouling properties of zwitterionic materials. Journal of the American Chemical Society, 2005. **127**(41): p. 14473-14478.

47. Mohamed, H., et al., Effects of charge and hydrophilicity on the anti-fouling properties of kidney-inspired, polyester membranes. Molecular Systems Design & Engineering, 2020. **5**(7): p. 1219-1229.

48. Unsworth, L.D., H. Sheardown, and J.L. Brash, Protein-resistant poly (ethylene oxide)-grafted surfaces: chain density-dependent multiple mechanisms of action. Langmuir, 2008. **24**(5): p. 1924-1929.

49. Unsworth, L.D., et al., Chemisorption of thiolated poly (ethylene oxide) to gold: surface chain densities measured by ellipsometry and neutron reflectometry. Journal of colloid and interface science, 2005. **281**(1): p. 112-121.

50. Du, Y.J., PEO and PEO-heparin modified surfaces for blood contacting applications. 2004: National Library of Canada= Bibliothèque nationale du Canada, Ottawa.

51. Benesch, J., et al., Protein adsorption to oligo (ethylene glycol) self-assembled monolayers: experiments with fibrinogen, heparinized plasma, and serum. Journal of Biomaterials Science, Polymer Edition, 2001. **12**(6): p. 581-597.

52. Fang and I. Szleifer, Effect of molecular structure on the adsorption of protein on surfaces with grafted polymers. Langmuir, 2002. **18**(14): p. 5497-5510.

53. Satulovsky, J., M. Carignano, and I. Szleifer, Kinetic and thermodynamic control of protein adsorption. Proceedings of the National Academy of Sciences, 2000. **97**(16): p. 9037-9041.

54. Israelachvili, J. and H. Wennerström, Role of hydration and water structure in biological and colloidal interactions. Nature, 1996. **379**(6562): p. 219-225.

55. Batteas, J.D., Biopolymers at Interfaces Edited by Martin Malmsten (Institute for Surface Chemistry, Stockholm, Sweden). Surfactant Science Series, Vol. 75. Marcel Dekker: New York. 1998. x+ 680 pp. $235.00. ISBN 0-8247-0201-8. 1999, ACS Publications.

56. Burns, N.L., J.M. Van Alstine, and J.M. Harris, Poly (ethylene glycol) grafted to quartz: analysis in terms of a site-dissociation model of electroosmotic fluid flow. Langmuir, 1995. **11**(7): p. 2768-2776.

57. Feldman, K., et al., Probing resistance to protein adsorption of oligo (ethylene glycol)-terminated self-assembled monolayers by scanning force microscopy. Journal of the American Chemical Society, 1999. **121**(43): p. 10134-10141.

58. Dicke, C. and G. Hähner, pH-Dependent force spectroscopy of tri (ethylene glycol)-and methyl-terminated self-assembled monolayers adsorbed on gold. Journal of the American Chemical Society, 2002. **124**(42): p. 12619-12625.

59. Dicke, C. and G. Hähner, Interaction between a hydrophobic probe and tri (ethylene glycol)-containing self-assembled monolayers on gold studied with force spectroscopy in aqueous electrolyte solution. The Journal of Physical Chemistry B, 2002. **106**(17): p. 4450-4456.

60. Wang, R.L., H.J. Kreuzer, and M. Grunze, The interaction of oligo (ethylene oxide) with water: a quantum mechanical study. Physical Chemistry Chemical Physics, 2000. **2**(16): p. 3613-3622.

61. Zolk, M., et al., Solvation of oligo (ethylene glycol)-terminated self-assembled monolayers studied by vibrational sum frequency spectroscopy. Langmuir, 2000. **16**(14): p. 5849-5852.

62. Kingshott, P., et al., Ultrasensitive probing of the protein resistance of PEG surfaces by secondary ion mass spectrometry. Biomaterials, 2002. **23**(24): p. 4775-4785.

63. Molineux, P., Water soluble synthetic polymers; properties and behavior. 1983, CRC Press: Boca Raton, FL.

64. Jones, R.A. and R.W. Richards, Polymers at surfaces and interfaces. 1999.

65. Sofia, S.J. and E.W. Merrill, Protein adsorption on poly (ethylene oxide)-grafted silicon surfaces. 1997, ACS Publications.

66. Murray, I. and M.A. Paolini, Histology, kidney and glomerulus. 2020.

67. Wiggins, R.-C., The spectrum of podocytopathies: a unifying view of glomerular diseases. Kidney international, 2007. **71**(12): p. 1205-1214.

68. Jegatheswaran, J., et al., Anticoagulation in patients with advanced chronic kidney disease: walking the fine line between benefit and harm. Canadian Journal of Cardiology, 2019. **35**(9): p. 1241-1255.

69. Li, S., et al., Adsorption Dynamics of Uremic Toxins to Novel Modified Magnetic Nanoparticles. Macromolecular Bioscience, 2024. **24**(2): p. 2300133.

70. Ma, Y., et al., Adsorption-based strategies for removing uremic toxins from blood. Microporous and Mesoporous Materials, 2021. **319**: p. 111035.

71. Kam-Tao Li, P., et al., Kidney health for everyone everywhere-from prevention to detection and equitable access to care. Nephrology and Dialysis, 2020. **22**(1): p. 10-23.

72. Tarun, T., et al., Updates on new therapies for patients with CKD. Kidney International Reports, 2023.

73. Cockwell, P. and L.-A. Fisher, The global burden of chronic kidney disease. The Lancet, 2020. **395**(10225): p. 662-664.

74. Shlipak, M.G., et al., Elevations of inflammatory and procoagulant biomarkers in elderly persons with renal insufficiency. Circulation, 2003. **107**(1): p. 87-92.

75. Lutz, J., et al., Haemostasis in chronic kidney disease. Nephrology Dialysis Transplantation, 2014. **29**(1): p. 29-40.

76. Espi, M., et al., Chronic kidney disease-associated immune dysfunctions: impact of protein-bound uremic retention solutes on immune cells. Toxins, 2020. **12**(5): p. 300.

77. Li, S., M. Tonelli, and L.D. Unsworth, Indoxyl and p-cresol sulfate binding with human serum albumin. Colloids and Surfaces A: Physicochemical and Engineering Aspects, 2022. **635**: p. 128042.

78. Shi, Y., et al., Increasing the removal of protein-bound uremic toxins by liposome-supported hemodialysis. Artificial organs, 2019. **43**(5): p. 490-503.

79. Duranton, F., et al., Normal and pathologic concentrations of uremic toxins. Journal of the American Society of Nephrology, 2012. **23**(7): p. 1258-1270.

80. Vanholder, R., et al., Review on uremic toxins: classification, concentration, and interindividual variability. Kidney international, 2003. **63**(5): p. 1934-1943.

81. Peter, B., et al., Green tea polyphenol tailors cell adhesivity of RGD displaying surfaces: multicomponent models monitored optically. Scientific Reports, 2017. **7**(1): p. 42220.

82. Prapainop, K., D.P. Witter, and P. Wentworth Jr, A chemical approach for cell-specific targeting of nanomaterials: small-molecule-initiated misfolding of nanoparticle corona proteins. Journal of the American Chemical Society, 2012. **134**(9): p. 4100-4103.

83. Sánchez-Ospina, D., et al., Displacing the Burden: A Review of Protein-Bound Uremic Toxin Clearance Strategies in Chronic Kidney Disease. Journal of Clinical Medicine, 2024. **13**(5): p. 1428.

84. Kurbatov, I., et al., The knowns and unknowns in protein–metabolite interactions. International Journal of Molecular Sciences, 2023. **24**(4): p. 4155.

85. Luzarowski, M., et al., Global mapping of protein–metabolite interactions in Saccharomyces cerevisiae reveals that Ser-Leu dipeptide regulates phosphoglycerate kinase activity. Communications biology, 2021. **4**(1): p. 181.

86. Gorisse, L., et al., Carbamylated proteins in renal disease: aggravating factors or just biomarkers? International journal of molecular sciences, 2022. **23**(1): p. 574.

87. Ma, Y., Engineered surfaces for binding carbamylated proteins. 2021.

88. Bacal, C.J.O., et al., Fouling during hemodialysis–Influence of module design and membrane surface chemistry. Advanced Membranes, 2024: p. 100100.

89. Cicco, S.R., et al., Improving the In Vitro Removal of Indoxyl Sulfate and p-Cresyl Sulfate by Coating Diatomaceous Earth (DE) and Poly-vinyl-pyrrolidone-co-styrene (PVP-co-S) with Polydopamine. Toxins, 2022. **14**(12): p. 864.

90. Nguyen, C.H., et al., Enhanced and selective adsorption of urea and creatinine on amine-functionalized mesoporous silica SBA-15 via hydrogen bonding. Microporous and Mesoporous Materials, 2021. **311**: p. 110733.

91. Kharina, A. and T. Eliseeva, Tyrosine Amino Acid as a Foulant for the Heterogeneous Anion Exchange Membrane. Membranes, 2023. **13**(10): p. 844.

92. Erol, K., et al., Electrostatic adsorption of asymmetric dimethyl arginine (adma) on poly (2-hydroxyethyl methacrylate-acrylic acid) nanoparticles. Journal of Macromolecular Science, Part A, 2017. **54**(12): p. 902-907.

93. Penfold, J., R. Thomas, and P. Li, Biogenic amine–Surfactant interactions at the air–water interface. Journal of colloid and interface science, 2015. **449**: p. 167-174.

94. Kijima, T., Y. Sekikawa, and S. Ueno, Adsorption of L-asparagine and L-alanine on α-zirconium phosphate. Journal of Inorganic and Nuclear Chemistry, 1981. **43**(4): p. 849-853.

95. Guangle, Q., et al., Adsorption of uremic toxins by modified activated carbon of different mesh with sulfuric acid. Adsorption, 2024: p. 1-12.

96. Clark, A., The chemisorptive bond: Basic concepts. Vol. 32. 2012: Elsevier.

97. Webb, P.A., Introduction to chemical adsorption analytical techniques and their applications to catalysis. MIC Tech. Publ, 2003. **13**: p. 1-4.

98. Sellers, H., et al., Structure and binding of alkanethiolates on gold and silver surfaces: implications for self-assembled monolayers. Journal of the American Chemical Society, 1993. **115**(21): p. 9389-9401.

99. Borzenkov, M., et al., Thermal and chemical stability of thiol bonding on gold nanostars. Langmuir, 2015. **31**(29): p. 8081-8091.

100. Cristina, L.J., et al., Thermal stability of self-assembled monolayers of n-Hexanethiol on Au (111)-(1× 1) and Au (001)-(1× 1). The Journal of Physical Chemistry C, 2017. **121**(50): p. 27894-27904.

101. Kingshott, P. and H.J. Griesser, Surfaces that resist bioadhesion. Current Opinion in Solid State and Materials Science, 1999. **4**(4): p. 403-412.

102. Kingshott, P., H. Thissen, and H.J. Griesser, Effects of cloud-point grafting, chain length, and density of PEG layers on competitive adsorption of ocular proteins. Biomaterials, 2002. **23**(9): p. 2043-2056.

103. Vuckovac, M., et al., Uncertainties in contact angle goniometry. Soft Matter, 2019. **15**(35): p. 7089-7096.

104. Kamaraj, A.B., V. Shaw, and M.M. Sundaram, Novel fabrication of un-coated super-hydrophobic aluminum via pulsed electrochemical surface modification. Procedia Manufacturing, 2015. **1**: p. 892-903.

105. Airaksinen, V.-M., Silicon wafer and thin film measurements, in Handbook of silicon based MEMS materials and technologies. 2015, Elsevier. p. 381-390.

106. Jungk, G., Possibilities and limitations of ellipsometry. Thin Solid Films, 1993. **234**(1-2): p. 428-431.

107. Politano, G.G. and C. Versace, Spectroscopic Ellipsometry: Advancements, Applications and Future Prospects in Optical Characterization. Spectroscopy Journal, 2023. **1**(3): p. 163-181.

108. Fujiwara, H., Spectroscopic ellipsometry: principles and applications. 2007: John Wiley & Sons.

109. Lefebvre, J., et al., Experimental methods in chemical engineering: X-ray photoelectron spectroscopy-XPS. The Canadian Journal of Chemical Engineering, 2019. **97**(10): p. 2588-2593.

110. Fadley, C.S., Atomic-level characterization of materials with core-and valence-level photoemission: basic phenomena and future directions. Surface and Interface Analysis: An International Journal devoted to the development and application of techniques for the analysis of surfaces, interfaces and thin films, 2008. **40**(13): p. 1579-1605.

111. Krishna, D.N.G. and J. Philip, Review on surface-characterization applications of X-ray photoelectron spectroscopy (XPS): Recent developments and challenges. Applied Surface Science Advances, 2022. **12**: p. 100332.

112. Patel, D.I., et al., Introduction to near-ambient pressure x-ray photoelectron spectroscopy characterization of various materials. Surface Science Spectra, 2019. **26**(1).

113. Hofer, F., et al. Fundamentals of electron energy-loss spectroscopy. in IOP conference series: Materials science and engineering. 2016. IOP Publishing.

114. Ebnesajjad, S. and C. Ebnesajjad, Surface treatment of materials for adhesive bonding. 2013: William Andrew.

115. Ortega, R., et al., X-ray absorption spectroscopy of biological samples. A tutorial. Journal of Analytical Atomic Spectrometry, 2012. **27**(12): p. 2054-2065.

116. Eslami, A. and J. Lujan, Western blotting: sample preparation to detection. JoVE (Journal of Visualized Experiments), 2010(44): p. e2359.

117. Gallagher, S., et al., Immunoblotting and immunodetection. Current protocols in cell biology, 2011. **52**(1): p. 6.2. 1-6.2. 28.

118. Laemmli, U.K., Cleavage of structural proteins during the assembly of the head of bacteriophage T4. nature, 1970. **227**(5259): p. 680-685.

119. Gavini, K. and K. Parameshwaran, Western blot. 2019.

120. Harlow, E. and D. Lane, Immunoblotting: preparing protein solutions. Cold Spring Harbor Protocols, 2006. **2006**(3): p. pdb. prot4298.

121. Green, M.R. and J. Sambrook, Polyacrylamide gel electrophoresis. Cold Spring Harbor Protocols, 2020. **2020**(12): p. pdb. prot100412.

122. Brunelle, J.L. and R. Green, One-dimensional SDS-polyacrylamide gel electrophoresis (1D SDS-PAGE), in Methods in enzymology. 2014, Elsevier. p. 151-159.

123. Kurien, B.T. and R.H. Scofield, Western blotting: an introduction. Western blotting: Methods and protocols, 2015: p. 17-30.

124. Kurien, B.T., et al., SDS-PAGE to immunoblot in one hour. Western Blotting: Methods and Protocols, 2015: p. 449-454.

125. Madamanchi, N.R. and M.S. Runge, Western blotting. Angiotensin Protocols, 2001: p. 245-256.

126. Taylor, S.C. and A. Posch, The design of a quantitative western blot experiment. BioMed research international, 2014. **2014**(1): p. 361590.

127. Pillai-Kastoori, L., A.R. Schutz-Geschwender, and J.A. Harford, A systematic approach to quantitative Western blot analysis. Analytical biochemistry, 2020. **593**: p. 113608.

128. Ghosh, R., J.E. Gilda, and A.V. Gomes, The necessity of and strategies for improving confidence in the accuracy of western blots. Expert review of proteomics, 2014. **11**(5): p. 549-560.

129. Lück, C., C. Haitjema, and C. Heger, Simple Western: Bringing the Western blot into the twenty-first century. Proteomic Profiling: Methods and Protocols, 2021: p. 481-488.

130. Meftahi, G.H., et al., Applications of western blot technique: From bench to bedside. Biochemistry and Molecular Biology Education, 2021. **49**(4): p. 509-517.

131. Du, Y., R. Cornelius, and J. Brash, Measurement of protein adsorption to gold surface by radioiodination methods: suppression of free iodide sorption. Colloids and Surfaces B: Biointerfaces, 2000. **17**(1): p. 59-67.

132. Cornelius, R.M., et al., Adsorption of proteins from infant and adult plasma to biomaterial surfaces. Journal of Biomedical Materials Research: An Official Journal of The Society for Biomaterials, The Japanese Society for Biomaterials, and The Australian Society for Biomaterials and the Korean Society for Biomaterials, 2002. **60**(4): p. 622-632.

133. Ren, C.-l., et al., Molecular and thermodynamic factors explain the passivation properties of poly (ethylene glycol)-coated substrate surfaces against fluorophore-labeled DNA oligonucleotides. Langmuir, 2015. **31**(42): p. 11491-11501.

134. Lv, J., et al., Effect of end-grafted PEG conformation on the hemocompatibility of poly (styrene-b-(ethylene-co-butylene)-b-styrene). Journal of Biomaterials Science, Polymer Edition, 2019. **30**(17): p. 1670-1685.

135. Pertsin, A.J., T. Hayashi, and M. Grunze, Grand canonical Monte Carlo Simulations of the hydration interaction between oligo (ethylene glycol)-terminated alkanethiol self-

assembled monolayers. The Journal of Physical Chemistry B, 2002. **106**(47): p. 12274-12281.

136. Alexander, S., Adsorption of chain molecules with a polar head a scaling description. Journal De Physique, 1977. **38**(8): p. 983-987.

137. Yi, L., et al., New protein-resistant surfaces of amphiphilic graft copolymers containing hydrophilic poly (ethylene glycol) and low surface energy fluorosiloxane side-chains. Applied Surface Science, 2019. **480**: p. 923-933.

138. Hu, Y., et al., Study of fibrinogen adsorption on poly (ethylene glycol)-modified surfaces using a quartz crystal microbalance with dissipation and a dual polarization interferometry. Rsc Advances, 2014. **4**(15): p. 7716-7724.

139. Kuchinka, J., et al., Control of blood coagulation by hemocompatible material surfaces—a review. Bioengineering, 2021. **8**(12): p. 215.

140. Nonckreman, C.J., et al., Competitive adsorption of fibrinogen and albumin and blood platelet adhesion on surfaces modified with nanoparticles and/or PEO. Colloids and Surfaces B: Biointerfaces, 2010. **77**(2): p. 139-149.

141. Amiji, M. and K. Park, Prevention of protein adsorption and platelet adhesion on surfaces by PEO/PPO/PEO triblock copolymers. Biomaterials, 1992. **13**(10): p. 682-692.

142. Sasaki, M., Y. Liu, and M. Ebara, Zeolite composite nanofiber mesh for indoxyl sulfate adsorption toward wearable blood purification devices. Fibers, 2021. **9**(6): p. 37.

143. Itoh, Y., et al., Protein-bound uremic toxins in hemodialysis patients measured by liquid chromatography/tandem mass spectrometry and their effects on endothelial ROS production. Analytical and bioanalytical chemistry, 2012. **403**: p. 1841-1850.

144. Kopple, J.D., et al., The free and bound amino acids removed by hemodialysis. ASAIO Journal, 1973. **19**(1): p. 309-313.

145. Canepa, A., et al., Free amino acids in plasma, red blood cells, polymorphonuclear leukocytes, and muscle in normal and uraemic children. Nephrology Dialysis Transplantation, 2002. **17**(3): p. 413-421.

146. Landon, J., J. Fawcett, and V. Wynn, Blood pyruvate concentration measured by a specific method in control subjects. Journal of clinical pathology, 1962. **15**(6): p. 579-584.

147. Bain, M.A., et al., Accumulation of trimethylamine and trimethylamine-N-oxide in end-stage renal disease patients undergoing haemodialysis. Nephrology Dialysis Transplantation, 2006. **21**(5): p. 1300-1304.

148. Taki, K., Y. Tsuruta, and T. Niwa, Indoxyl sulfate and atherosclerotic risk factors in hemodialysis patients. American Journal of Nephrology, 2007. **27**(1): p. 30-35.

149. Toshimitsu, N., T. Naohito, and Y. Hideo, RNA metabolism in uremic patients: accumulation of modified ribonucleosides in uremic serum. Kidney Int, 1998. **53**: p. 1801-1806.

150. Schools, A., et al., Biochemical and neurophysiological parameters in hemodialyzed patients with chronic renal failure. Clinica chimica acta, 1989. **185**(1): p. 91-107.

151. Wolfson, M., M.R. Jones, and J.D. Kopple, Amino acid losses during hemodialysis with infusion of amino acids and glucose. Kidney international, 1982. **21**(3): p. 500-506.

152. Du, Y.J. and J.L. Brash, Synthesis and characterization of thiol-terminated poly (ethylene oxide) for chemisorption to gold surface. Journal of applied polymer science, 2003. **90**(2): p. 594-607.

153. Harder, P., et al., Molecular conformation in oligo (ethylene glycol)-terminated self-assembled monolayers on gold and silver surfaces determines their ability to resist protein adsorption. The Journal of Physical Chemistry B, 1998. **102**(2): p. 426-436.

154. Troughton, E.B., et al., Monolayer films prepared by the spontaneous self-assembly of symmetrical and unsymmetrical dialkyl sulfides from solution onto gold substrates: structure, properties, and reactivity of constituent functional groups. Langmuir, 1988. **4**(2): p. 365-385.

155. Klok, O., A. Igual Munoz, and S. Mischler, An overview of serum albumin interactions with biomedical alloys. Materials, 2020. **13**(21): p. 4858.

156. Wu, Y., Contact pathway of coagulation and inflammation. Thrombosis journal, 2015. **13**: p. 1-9.

157. Dahlbäck, B.r. and B.O. Villoutreix, Regulation of blood coagulation by the protein C anticoagulant pathway: novel insights into structure-function relationships and molecular recognition. Arteriosclerosis, thrombosis, and vascular biology, 2005. **25**(7): p. 1311-1320.

158. Wang, Y., et al., Plasma fibronectin supports hemostasis and regulates thrombosis. The Journal of clinical investigation, 2014. **124**(10): p. 4281-4293.

159. Molina, H., Complement and immunity. Rheumatic Disease Clinics, 2004. **30**(1): p. 1-18.

160. Ortega, V.A., et al., Polymer-coated nanoparticle protein corona formation potentiates phagocytosis of bacteria by innate immune cells and inhibits coagulation in human plasma. Biointerphases, 2020. **15**(5).

161. Bahniuk, M.S., A.K. Alshememry, and L.D. Unsworth, Human plasma protein adsorption to elastin-like polypeptide nanoparticles. Biointerphases, 2020. **15**(2).

162. Tan, J. and J. Brash, Nonfouling biomaterials based on polyethylene oxide-containing amphiphilic triblock copolymers as surface modifying additives: Adsorption of proteins from human plasma to copolymer/polyurethane blends. Journal of Biomedical Materials Research Part A: An Official Journal of The Society for Biomaterials, The Japanese Society for Biomaterials, and The Australian Society for Biomaterials and the Korean Society for Biomaterials, 2009. **90**(1): p. 196-204.

163. Moos, T. and E.H. Morgan, Transferrin and transferrin receptor function in brain barrier systems. Cellular and molecular neurobiology, 2000. **20**: p. 77-95.

164. Stafford, J.L. and M. Belosevic, Transferrin and the innate immune response of fish: identification of a novel mechanism of macrophage activation. Developmental & Comparative Immunology, 2003. **27**(6-7): p. 539-554.

165. Gresele, P., et al., Platelets in thrombotic and non-thrombotic disorders: pathophysiology, pharmacology and therapeutics. Journal of Thrombosis and Haemostasis, 2003. **1**(3): p. 613-614.

166. Bale, M.D., et al., Identification of vitronectin as a major plasma protein adsorbed on polymer surfaces of different copolymer composition. 1989.

167. Gunkel, G., et al., Effect of polymer brush architecture on antibiofouling properties. Biomacromolecules, 2011. **12**(11): p. 4169-4172.

168. Shen, Y.-x., et al., Biomimetic membranes: A review. Journal of Membrane Science, 2014. **454**: p. 359-381.

169. Hou, X., Liquid gating membrane. National Science Review, 2020. **7**(1): p. 9-11.

170. Kato, S., et al., Zirconium-based metal–organic frameworks for the removal of protein-bound uremic toxin from human serum albumin. Journal of the American Chemical Society, 2019. **141**(6): p. 2568-2576.

171. Said, N., et al., A review of commercial developments and recent laboratory research of dialyzers and membranes for hemodialysis application. Membranes, 2021. **11**(10): p. 767.

172. Rodrigues, F.S. and M. Faria, Adsorption-and displacement-based approaches for the removal of protein-bound uremic toxins. Toxins, 2023. **15**(2): p. 110.

173. Kratz, F., Albumin as a drug carrier: design of prodrugs, drug conjugates and nanoparticles. Journal of controlled release, 2008. **132**(3): p. 171-183.

174. Niwa, T., Uremic toxicity of indoxyl sulfate. Nagoya J Med Sci, 2010. **72**(1-2): p. 1-11.

175. Viaene, L., et al., Albumin is the main plasma binding protein for indoxyl sulfate and p-cresyl sulfate. Biopharmaceutics & drug disposition, 2013. **34**(3): p. 165-175.

176. Devine, E., et al., Binding affinity and capacity for the uremic toxin indoxyl sulfate. Toxins, 2014. **6**(2): p. 416-429.

177. Pitek, A.S., et al., Transferrin coated nanoparticles: study of the bionano interface in human plasma. PloS one, 2012. **7**(7): p. e40685.

178. Stoller, J.K. and L.S. Aboussouan, α1-antitrypsin deficiency. The Lancet, 2005. **365**(9478): p. 2225-2236.

179. Armstrong, P.B. and J.P. Quigley, α2-macroglobulin: an evolutionarily conserved arm of the innate immune system. Developmental & Comparative Immunology, 1999. **23**(4-5): p. 375-390.

180. Vandooren, J. and Y. Itoh, Alpha-2-macroglobulin in inflammation, immunity and infections. Frontiers in Immunology, 2021. **12**: p. 803244.

181. Bahniuk, M.S., et al., Bioactive glass 45S5 powders: effect of synthesis route and resultant surface chemistry and crystallinity on protein adsorption from human plasma. Biointerphases, 2012. **7**(1).

182. Pilli, V., W. Plautz, and R. Majumder, The journey of protein S from an anticoagulant to a signaling molecule. JSM biochemistry and molecular biology, 2016. **3**(1).

183. To, W.S. and K.S. Midwood, Plasma and cellular fibronectin: distinct and independent functions during tissue repair. Fibrogenesis & tissue repair, 2011. **4**: p. 1-17.

184. Davie, E.W. and J.D. Kulman. An overview of the structure and function of thrombin. in Seminars in thrombosis and hemostasis. 2006. Copyright© 2006 by Thieme Medical Publishers, Inc., 333 Seventh Avenue, New ….

185. McClung, W., et al., Lysine-derivatized polyurethane as a clot lysing surface: conversion of adsorbed plasminogen to plasmin and clot lysis in vitro. Biomaterials, 2001. **22**(13): p. 1919-1924.

186. McClung, W., et al., Adsorption of plasminogen from human plasma to lysine-containing surfaces. Journal of Biomedical Materials Research: An Official Journal of The Society for Biomaterials and The Japanese Society for Biomaterials, 2000. **49**(3): p. 409-414.

Appendix A. Supplemental information for Effect of uremic toxins and methoxy-PEO chain density on plasma protein adsorption

Aishwarya S. Pawar, Ayda Ghahremanzadeh, Mehdi Ghaffari Sharaf, Larry D. Unsworth*

Department of Chemical and Materials Engineering, University of Alberta, Edmonton, AB T6G 2V4, Canada

* Correspondence: Department of Chemical and Materials Engineering, University of Alberta, Edmonton, AB T6G 2V4, Canada; lunswort@ualberta.ca

Keywords: chronic kidney disease, protein adsorption, polyethylene oxide, uremic toxins, polymer chain densities, gold-coated silicon chips

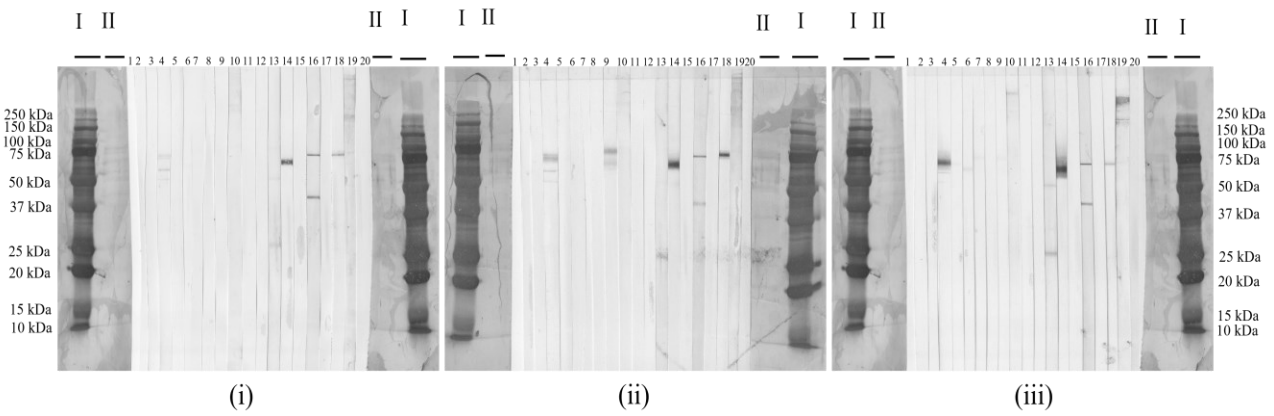

Figure A1. A reassembled immunoblot membrane illustrating plasma proteins. (i) PEO 10 min surfaces in normal plasma, (ii) PEO 4 hr surfaces in normal plasma, (iii) PEO 30 min surfaces in UTX plasma. The terminal strips represent colloidal gold-stained pieces of immunoblots, and the middle lanes (1-20) represent sample strips specific to individual proteins.

I Ladder

II Gold-stained protein samples

1 Ani-kininogen (light)

2 Ani-kininogen (heavy)

3 Anti-factor I

4 Anti-fibrinogen α, β, and γ

5 Anti-fibronectin

6 Anti- α_1 antitrypsin

7 Anti-prothrombin

8 Anti-protein C

9 Anti-vitronectin

10 Anti-protein S

11 Anti-prekallikrein

12 Anti-antithrombin

13 Anti-IgG

14 Anti-human serum albumin

15 Anti-plasminogen

16 Anti-C3

17 Anti-factor XII

18 Anti-factor XI

19 Anti-transferrin

20 Anti-α_2 macroglobulin

Table A1. Plasma protein-specific primary antibodies.

Anti-Human Plasma Antibody	Host	Supplier
Kininogen light chain	Mouse	US Biological, Swampscott, MA, USA
Kininogen heavy chain	Mouse	US Biological, Swampscott, MA, USA
Factor I	Mouse	Invitrogen; Thermo Fisher Scientific Inc.
Fibrinogen	Rabbit	Calbiochem, Gibbstown, NJ, USA
Fibronectin	Rabbit	Cedarlane Laboratories, Ontario, Canada
α_1 antitrypsin	Sheep	Cedarlane Laboratories, Ontario, Canada
Prothrombin	Sheep	Cedarlane Laboratories, Ontario, Canada
Protein C	Sheep	Cedarlane Laboratories, Ontario, Canada
Vitronectin	Sheep	Cedarlane Laboratories, Ontario, Canada
Protein S	Sheep	Cedarlane Laboratories, Ontario, Canada
Prekallikrein	Sheep	Cedarlane Laboratories, Ontario, Canada
Antithrombin	Sheep	Cedarlane Laboratories, Ontario, Canada
IgG	Goat	Sigma-Aldrich, MO,USA
Albumin	Goat	OEM Concepts, ME, USA
Plasminogen	Goat	Cedarlane Laboratories, Ontario, Canada
Complement factor 3	Goat	Calbiochem, NJ, USA
Factor XII	Goat	Cedarlane Laboratories, Ontario, Canada
Factor XI	Goat	Cedarlane Laboratories, Ontario, Canada
Transferrin	Goat	Sigma-Aldrich, MO, USA
α_2 macroglobulin	Goat	Sigma-Aldrich, MO, USA

Appendix B. Supplemental information for Effect of hydroxy-PEO chain density and uremic toxins on plasma protein adsorption

Aishwarya S. Pawar, Ayda Ghahremanzadeh, Mehdi Ghaffari Sharaf, Larry D. Unsworth*

Department of Chemical and Materials Engineering, University of Alberta, Edmonton, AB T6G 2V4, Canada.

* Correspondence: Department of Chemical and Materials Engineering, University of Alberta, Edmonton, AB T6G 2V4, Canada; lunswort@ualberta.ca

Keywords: protein adsorption, polyethylene oxide, polymer chain densities, uremic toxins, chronic kidney disease, gold-coated silicon chips

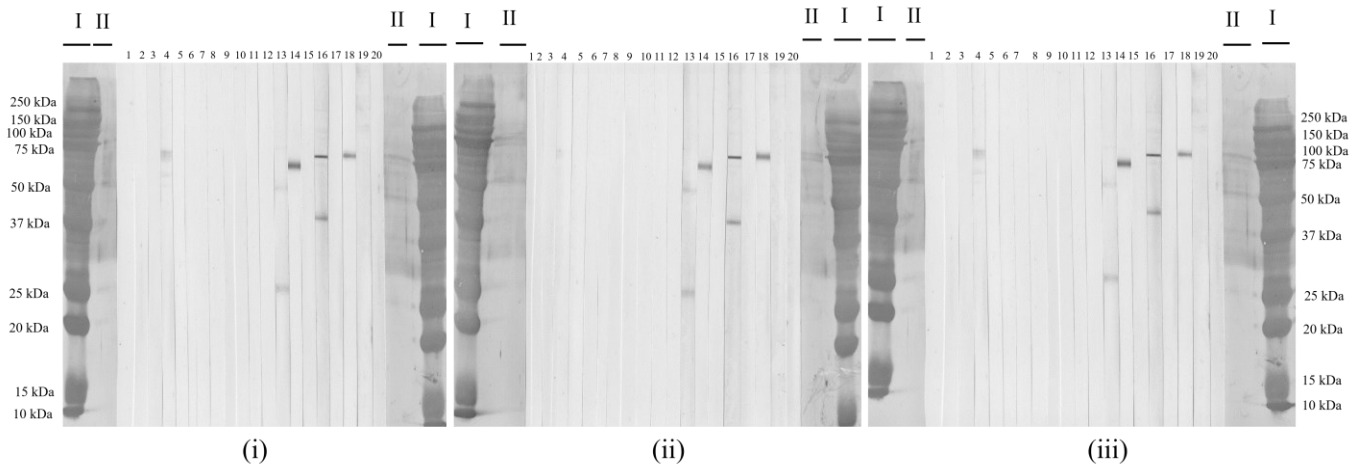

Figure B1. Individual protein bands illustrated by reassembled immunoblot membrane. (i) PEO 10 min surfaces in normal plasma, (ii) PEO 30 min surfaces in normal plasma, (iii) PEO 10 min surfaces in UTX plasma. Colloidal gold-stained strips occur at margins, and the sample strips in the middle (1-20) represent individual proteins.

I Ladder

II Gold-stained protein samples

1 Ani-kininogen (light)

2 Ani-kininogen (heavy)

3 Anti-factor I

4 Anti-fibrinogen α, β, and γ

5 Anti-fibronectin

6 Anti- α_1 antitrypsin

7 Anti-prothrombin

8 Anti-protein C

9 Anti-vitronectin

10 Anti-protein S

11 Anti-prekallikrein

12 Anti-antithrombin

13 Anti-IgG

14 Anti-human serum albumin

15 Anti-plasminogen

16 Anti-C3

17 Anti-factor XII

18 Anti-factor XI

19 Anti-transferrin

20 Anti-α_2 macroglobulin

Table B1. Plasma protein-specific primary antibodies.

Anti-Human Plasma Antibody	Host	Supplier
Kininogen light chain	Mouse	US Biological, Swampscott, MA, USA
Kininogen heavy chain	Mouse	US Biological, Swampscott, MA, USA
Factor I	Mouse	Invitrogen; Thermo Fisher Scientific Inc.
Fibrinogen	Rabbit	Calbiochem, Gibbstown, NJ, USA
Fibronectin	Rabbit	Cedarlane Laboratories, Ontario, Canada
α_1 antitrypsin	Sheep	Cedarlane Laboratories, Ontario, Canada
Prothrombin	Sheep	Cedarlane Laboratories, Ontario, Canada
Protein C	Sheep	Cedarlane Laboratories, Ontario, Canada
Vitronectin	Sheep	Cedarlane Laboratories, Ontario, Canada
Protein S	Sheep	Cedarlane Laboratories, Ontario, Canada
Prekallikrein	Sheep	Cedarlane Laboratories, Ontario, Canada
Antithrombin	Sheep	Cedarlane Laboratories, Ontario, Canada
IgG	Goat	Sigma-Aldrich, MO,USA
Albumin	Goat	OEM Concepts, ME, USA
Plasminogen	Goat	Cedarlane Laboratories, Ontario, Canada
Complement factor 3	Goat	Calbiochem, NJ, USA
Factor XII	Goat	Cedarlane Laboratories, Ontario, Canada
Factor XI	Goat	Cedarlane Laboratories, Ontario, Canada
Transferrin	Goat	Sigma-Aldrich, MO, USA
α_2 macroglobulin	Goat	Sigma-Aldrich, MO, USA

Appendix C. Western blotting protocol

Day 1: Plasma protein adsorption and elution

The protocol of incubation is modified from Unsworth et al. [36] and Markian Bahniuk [5].

1) 4 samples were considered for each PEO-modified system and clean, transparent, and non-adherent 96-well plates were used for plasma incubation of surfaces.
2) Individual surfaces were placed in 96-well plates, 200 µL of 37 ºC liquified plasma was filled in each well avoiding bubbles, and plates were incubated for 3 hrs at room temperature. For UTX plasma, previously prepared UTX vials were filled with 1 mL of liquified plasma each, mixed multiple times using a pipette, and left undisturbed at room temperature for 30 min.
3) The surfaces were transferred to different wells filled with 250 µL 1X (0.15 M) PBS each using soft tweezers (or fixing 1-10 µL pipette tips on normal tweezers). This was performed 3 times (10 minutes each) using fresh PBS each time to remove the residual plasma.
4) The inverted and cut 1.5 mL centrifuge tube and all 4 surfaces of the same sample type were placed in it, making sure they do not overlap. The surfaces were covered with 350 µL 2% SDS and incubated at room temperature overnight to elute the adsorbed proteome. Sonicate each elution system for 2 min, both before and after the elution, to obtain the best possible collection of adsorbed proteins. Collect the eluate the next morning and store at -80 ºC until use.

Day 2: SDS PAGE, Transfer, and Blocking

5) Prepare transfer buffer as follows and store it at 4 ºC until use.

Transfer Buffer:

Methanol	200 mL
Tris Base	3 g
Glycine	14.4 g

Fill it to 1 L with Milli-Q water

6) Prepare the separating and stacking gels according to the Bio-Rad Mini-Protein® Tetra Cell Instruction Manual.

12% separating gel:

Milli-Q water	8.6 mL
40% Acrylamide	6 mL
1.5 M Tris HCL (pH 8.8)	5 mL
10% SDS	200 µL
10% Ammonium Persulfate	200 µL
TEMED	10 µL

Add the chemicals mentioned above in a sequence starting from Milli-Q water. Upon adding 10% APS and TEMED, gently mix the solution (avoiding bubbles) and fill in the gel plates IMMEDIATELY before it starts solidifying. Wait for 2 min and spray some Milli-Q water over the gels. Keep undisturbed for 30 min to solidify the gels.

4% stacking gel:

Milli-Q Water	5.5 mL
40% Acrylamide	938 µL
1.5 M Tris HCL (pH 6.8)	938 µL
10% SDS	75 µL
10% Ammonium Persulfate	75 µL
TEMED	10 µL

Upon adding 10% APS and TEMED, mix the gel contents gently. Pour off the water sprayed over separating gel and fill the stacking gel solution on the top of separating gel. Quickly insert the western blotting combs and allow the gel to solidify for 30 min.

7) Prepare the sample. For each gel, take 100 µL of eluted protein sample and add 1/3 of 4X sample buffer (~33 µL) to it. The total volume of sample for each gel should be optimized prior to the experiment.

Prepare the sample buffer (4X) as given below, aliquot and store at -20 ºC.

Milli-Q Water	6.35 mL
β-Mercaptoethanol	600 µL
10% Coomassie R250	50 µL
2M Tris pH 7.0	750 µL
SDS	1.2 g
100% Glycerol	3 mL

8) Followed by the addition of sample buffer to eluted protein sample, heat the mixture at 95 ^{o}C for 5 min.

9) Carefully remove the gel from the casting stand and fix it into the electrophoresis clamp, ensuring the shorter gel plates face inward. Fix the clamp in the buffer chamber and fill the chamber with 1X electrophoresis running buffer up to the indicated level. Using the gel loading pipettes, load 3 μL of ladder solution into first and last lanes of the gel, and sample in the large central lane. Close the lid and run the electrophoresis at 200 V and 400 mA until the dye approaches the bottom of the gel, which should take approximately ~35 min.

Electrophoresis running buffer (5X)

Tris Base	15 g
Glycine	72 g
SDS	5 g

Adjust the volume to 1 L with Milli-Q water. Prior to use, dilute to 1X with Milli-Q water.

10) Once gel electrophoresis is complete, transfer the gel to a transfer buffer and let it incubate with gentle agitation for 20 minutes.

11) Cut the Immobilon PVDF transfer membrane to the required size (use the size template), then pre-wet it by immersing it in 100% methanol for 3 seconds, followed by 1 minute in water, and finally incubate it in a transfer buffer for 15 minutes. Assemble the gel and membrane in the transfer cell as per the instructions. From the black plate of the transfer cell: foam pad, pre-wet filter paper, gel, PVDF membrane, pre-wet filter paper, and foam pad. Use forceps to handle the membranes, and never touch the PVDF membrane with bare

or gloved hands. Make sure to eliminate any trapped air bubbles between them, close the clamps, gently press using hands, and fix this assembly in a transfer chamber. An extra foam pad can be used to tighten the membrane sandwich. Fill the transfer chamber with transfer buffer to the indicated level, and perform the transfer for 1 hour at 100 V and 200 mA.

12) Following the transfer, mark a line at the bottom of the PVDF membrane for orientation and identification, especially if handling multiple blots. NEVER use a marker; use a point ball pen instead.
13) Cut two 1.5 cm strips containing a ladder from both edges of the membrane for gold staining. Cut 20 smaller strips (~2.5 mm) of the middle sample lane for blocking and subsequent immunoblotting. Do not block the gold staining strips.
14) Prepare a 5% Blocking solution by adding 5 g nonfat dry milk to 100 mL 1X TTBS buffer and filling 2 mL of this solution into each well of the Western plate.
15) Briefly pre-wet the sample strips in methanol for 3 seconds, then in water for 10 seconds, and subsequently place them into the wells of Western Plates containing blocking solution. Make sure the strips are completely immersed in the solution. Close the lids and incubate overnight at 4 ^{o}C with rocking.

Day 3: Immunoblotting and gold staining

16) Replace the blocking solution with 2 mL of washing solution (0.1% nonfat dry milk in 1X TBS buffer) using multichannel pipettes. Perform 3 washes, each lasting 10 min, and using fresh wash solution per wash.

Wash solution:

Nonfat dry milk	0.8 g
1X TBS buffer	800 mL

17) After this, fill the wells with 500 µL of primary antibodies (diluted 1:1000) and incubate for 3 hours at room temperature on a rocking platform.
18) Wash three times for 10 minutes each to remove loosely bound antibodies.
19) Expose the strips to 500 µL of secondary antibodies (diluted 1:1000) and incubate for 1 hour at room temperature with rocking. Make sure the strips are entirely covered by antibody solutions.
20) Repeat step 18 to remove loosely bound secondary antibodies, add 350 µL of TMB-stabilized HRP substrate to each well, and incubate with rocking at room temperature until precipitation begins. For consistency in comparing multiple blots, ensure uniform color development time, 15 min in the present study.
21) Replace the TMB solution with 2 mL of Milli-Q water and incubate for 10 minutes to terminate the reaction.
22) Dry the strips using a gel dryer, reassemble them, and scan them as soon as possible.
23) For gold staining of ladder strips, first wet them by immersing in methanol for 3 seconds, followed by Milli-Q water for 10 seconds.

24) Transfer the strip to a petri dish and cover it with enough TTBS solution. Incubate for 20 minutes to block the membrane on a rocking platform. Repeat this procedure two more times, using fresh TTBS for each incubation.
25) Immerse in Milli-Q water for 2 minutes, repeating three times, and add Colloidal Gold solution, ensuring it covers the strips. Incubate for 40-50 min based on the intensity of the gold nanoparticles with rocking at room temperature. Terminate the reaction when the protein bands are clearly visible and keep the gold solution for future use.
26) Rinse with Milli-Q water three times, each for 1 minute to remove the residual Colloidal Gold Solution. Let the membrane dry before incorporating it into the Western blot strips.

Important Western Blotting Solutions.

10X TBS:

Tris Base	60.57 g (500 M)
NaCl	87.66 g (1.5 M)
Milli-Q Water	900 mL

Adjust pH to 7.4, make the final volume up to 1 L with Milli-Q Water, and filter sterilize.

1X TTBS:

10X TBS	100 mL
Tween 20	300 µL

Adjust the volume to 1 L with Milli-Q Water

Antibody Dilution Solution:

Nonfat dry milk	1 g
Tween 20	50 µL

1X TBS buffer	80 mL

Make total volume up to 100 mL using 1X TBS buffer.